Received: 4 September 2019 | Revised: 22 July 2020 | Accepted: 25 July 2020

DOI: 10.1111/bph.15231

RESEARCH PAPER

A novel histone deacetylase 6 inhibitor improves myelination of Schwann cells in a model of Charcot–Marie–Tooth disease type 1A

Nina Ha[1,2] | Young Il Choi[2] | Namhee Jung[3] | Ju Young Song[2] | Dae Kwon Bae[2] | Min Cheol Kim[2] | Yong Jae Lee[2] | Hyeseung Song[2] | Geon Kwak[1] | Soyeon Jeong[3] | Saeyoung Park[3] | Soo Hyun Nam[4] | Sung-Chul Jung[3] | Byung-Ok Choi[1,4]

[1]Department of Health Sciences and Technology, SAIHST, Sungkyunkwan University, Seoul, Republic of Korea

[2]CKD Research Institute, Yongin, Republic of Korea

[3]Department of Biochemistry, College of Medicine, Ewha Womans University, Seoul, Republic of Korea

[4]Department of Neurology, Samsung Medical Center, Sungkyunkwan University School of Medicine, Seoul, Republic of Korea

Correspondence
Byung-Ok Choi, Department of Neurology, Samsung Medical Center, Sungkyunkwan University School of Medicine, 81, Irwon-ro, Gangnam-gu, Seoul 06351, Republic of Korea.
Email: bochoi@skku.edu

Sung-Chul Jung, Department of Biochemistry, College of Medicine, Ewha Womans University, 25 Magokdong-ro-2-gil, Gangseo-gu, Seoul 07804, Republic of Korea.
Email: jungsc@ewha.ac.kr

Funding information
National Research Foundation, Republic of Korea, Grant/Award Numbers: NRF-2018R1A4A1024506, NRF-2017R1A2B2004699, NRF-2016R1A5A2007009; Korean Health Technology R&D Project, Ministry of Health & Welfare, Grant/Award Numbers: HI16C0426, HI14C3484; CKD Pharmaceuticals

Background and Purpose: Charcot–Marie–Tooth (CMT) disease is the most common hereditary peripheral neuropathy. CMT type 1A (CMT1A) accounts for approximately 50% of CMT patients and is linked to PMP22 gene duplication. Histone deacetylase-6 (HDAC6) has pleiotropic effects, such as regulating lipid homeostasis and cellular stress. Although HDAC6 has been regarded as a promising drug target for neurodegenerative diseases, its inhibition has not yet been tested in CMT1A. Here we have tested the therapeutic potential of CKD-504, a clinical stage HDAC6 inhibitor, in a mouse model of CMT1A

Experimental Approach: The potency and selectivity of CKD-504 was evaluated, using a HDAC enzyme panel assay and western blots. The therapeutic potential of CKD-504 was evaluated using behavioural testing and electrophysiological assessments in the C22 mouse model of CMT1A. PMP22 protein expression and aggregation were analysed in mesenchymal stem cell-derived Schwann cells from CMT1A patients and sciatic nerves from C22 mice.

Key Results: The HDAC6 inhibitor, CKD-504, modulated molecular chaperon proteins such as HSP90 and HSP70, which are involved in the folding/refolding of proteins such as PMP22. CKD-504 treatment restored myelination in both mesenchymal stem cell-derived Schwann cells from CMT1A patients and sciatic nerves of C22 mice and improved the axonal integrity of the sciatic nerve, leading to behavioural, electrophysiological, and histological improvements in C22 mice.

Conclusion and Implications: A novel HDAC6 inhibitor, CKD-504, has potent therapeutic efficacy for CMT1A.

KEYWORDS

Charcot–Marie–Tooth disease, CKD-504, HDAC6, HSP90, PMP22

Abbreviations: AMC, 7-amino-4-methylcoumarin; CMAP, compound motor action potential; CMT, Charcot–Marie–Tooth disease; DRG, dorsal root ganglion; MNCV, motor neuron conduction velocity; PMP22, peripheral myelin protein; TCR, T cell receptor; UPR, unfolded protein response.

1 | INTRODUCTION

Charcot–Marie–Tooth (CMT) disease is the most common hereditary peripheral neuropathy, affecting about 1 in 2,500 persons (Skre, 1974). So far, mutations in more than 90 genes have been reported to cause CMT (Pareyson, Saveri, & Pisciotta, 2017; Timmerman, Strickland, & Zuchner, 2014). CMT type 1A (CMT1A), the major subtype, accounts for approximately 50% of all CMT cases and is associated with a duplication of the gene encoding peripheral myelin protein 22 (PMP22). PMP22 is an intrinsic membrane protein of myelin that is developmentally induced in Schwann cells when myelination is initiated in peripheral nerves (Timmerman et al., 2014). PMP22 overexpression causes extensive demyelination of peripheral nerves.

Histone deacetylase 6 (**HDAC6**) is a member of the HDAC family, which is divided into five subgroups (class I, class IIa, class IIb, class III, and class IV) based on the protein domain structures and functions. HDAC enzymes remove acetyl groups from the acetylated ε-amino groups of lysine residues to increase the positive charge of proteins and control protein interactions (Boyault, Sadoul, Pabion, & Khochbin, 2007; de Ruijter, van Gennip, Caron, Kemp, & van Kuilenburg, 2003; Gregoretti, Lee, & Goodson, 2004). HDAC6 is found mainly in cytosol and controls the acetylation status of cytosolic proteins such as α-tubulin (Simoes-Pires et al., 2013) and **heat shock protein 90 (HSP90)** (Bali et al., 2005), but it can also control the acetylation of some nuclear proteins. Because HDAC6 has two nuclear export signal motifs and one nuclear localization signal motif, it was reported to shuttle between the nucleus and cytoplasm (Batchu, Brijmohan, & Advani, 2016). HDAC6 has a C-terminal zinc-finger ubiquitin-binding domain and two catalytic domains (deacetylase domains 1 and 2) (Boyault et al., 2007).

HDAC6 is an attractive drug target for neurodegenerative diseases because evidence for the therapeutic efficacy of its inhibition in such diseases is accumulating (Seidel, Schnekenburger, Dicato, & Diederich, 2015). Defective axonal transport is associated with various neurodegenerative diseases (De Vos & Hafezparast, 2017; Holzbaur & Scherer, 2011; Millecamps & Julien, 2013; Prior, Van Helleputte, Benoy, & Van Den Bosch, 2017). The inhibition or deletion of HDAC6 has been reported to reduce the pathogenesis of Alzheimer's disease, Parkinson's disease, Huntington's disease, chemotherapy-induced neuropathy, and axonal CMT neuropathy (Dompierre et al., 2007; Govindarajan et al., 2013; Krukowski et al., 2017; Ma et al., 2019; Rossaert & Van Den Bosch, 2020; Selenica et al., 2014; Taes et al., 2013; Van Hellelputte et al., 2018). In CMT type 2F (CMT2F) and CMT type 2D (CMT2D) models, in which defective axonal transport results from reduced microtubule stability, HDAC6 inhibition restored the acetylation of α-tubulin and axonal transport, restoring peripheral nerve function (Adalbert et al., 2020; Benoy et al., 2017, 2018; d'Ydewalle et al., 2011; Mo et al., 2018). However, the efficacy of HDAC6 inhibition in CMT1, which is a demyelinating neuropathy, has not yet been reported.

The aim of this study was to evaluate the therapeutic potential of CKD-504 in vitro in a differentiation model using mesenchymal stem cell (MSC) derived Schwann cells from CMT1A patients and in vivo in C22 mice, a previously established CMT1A animal model (Huxley et al., 1996).

What is already known

- HDAC6 inhibition induces protein refolding and degradation to reduce the stress from misfolded proteins.

What does this study add

- A selective inhibitor of HDAC6 reduces PMP22 protein expression and aggregation.
- Reduced PMP22 aggregation improves myelination of the sciatic nerve in a mouse model of CMT1A.

What is the clinical significance

- This study provides the rationale for accelerating the clinical development of CKD-504 for CMT1A.

2 | METHODS

2.1 | Enzyme assay

To evaluate the potency and selectivity of CKD-504, an HDAC panel assay was carried out by Reaction Biology Corp (PA, USA). Briefly, the deacetylation reaction was performed in 50 mM Tris–HCl (pH 8.0), 137 mM NaCl, 2.7 mM KCl, 1 mM $MgCl_2$, and 1 $mg{\cdot}ml^{-1}$ BSA with substrate. The substrate for each HDAC isoform was as follows: fluorogenic peptide from p53 residues 379–382 (RHKK-Ac-AMC) for HDAC1, 2, 3, 6, and 10; fluorogenic HDAC Class IIa substrate (trifluoroacetyl lysine) for HDAC4, 5, 7, 9, and 11; and fluorogenic peptide from p53 residues 379–382 (RHK-Ac-K-Ac-AMC) for HDAC8. After the reaction, a fluorescence signal (λEx360 nm/λEm460 nm) was developed (∼30 min) by the addition of an equal volume of trypsin/TSA solution. For the kinetic study against HDAC6, RHKK-Ac-AMC (Enzo Life Science) substrate, and CKD-504 were diluted to the desired concentrations (substrate: 1.56, 3.12, 6.25, 12.5, 25, and 50 μM; CKD-504: 0, 1.52, 4.57, 13.71, 41.15, and 123.45 nM). HDAC6 (0.042 μM, #382180, Calbiochem) and the diluted CKD-504 were mixed, and then the enzyme reaction was initiated by adding the pre-diluted substrates. The deacetylation reaction was stopped by adding trypsin/TSA solution. After 20 min of incubation, AMC release was monitored by measuring the fluorescence at λ_{Ex}360 nm/λ_{Em}460 nm using a microplate reader (Envision, PerkinElmer). The inhibition type and K_i value were determined based on a Michaelis–Menten plot

($V = V_{max}[S]/(K_M + [S])$) and double reciprocal plot or Lineweaver–Burk plot ($1/V = (K_M + [S])/V_{max}[S] = (K_M/V_{max})(1/[S]) + (1/V_{max})$) using GraphPad Prism 5.0 software (RRID:SCR_002798). Other kinetic parameters were calculated as described in Wegener, Wirsching, Riester, and Schwienhorst (2003). Here, V is the reaction velocity or reaction rate, K_M is the Michaelis–Menten constant, V_{max} is the maximum action velocity, and [S] is the substrate concentration. The HDAC panel assay and HDAC6 kinetic assay were repeated five times.

2.2 | Western blots

Human peripheral blood mononuclear cells (PBMCs) (IRB No. CKD-IRB-012) were seeded (1.0×10^6 cells per well) and cultured for 24 h on a 12-well plate before they were treated with CKD-504 or LBH-589 for 4 h. After harvesting the cells, total protein extracts were prepared and resolved in pre-made SDS-PAGE (NuPAGEÒ Bis-Tris Precast Gels, Invitrogen). Proteins were transferred onto a PVDF membrane and probed with the following antibodies: anti-acetyl α-tubulin (1:5,000) (Cell Signaling Technology, Cat# 5335, RRID:AB_10544694), anti-α-tubulin (1:2,000) (Cell Signaling Technology Cat# 2144, RRID:AB_2210548), anti-acetyl histone H4 (1:5,000) (Cell Signaling Technology Cat# 8647, RRID: AB_11217428), anti-histone H4 (1:1,000) (Cell Signaling Technology Cat# 2935, RRID:AB_1147658), anti-Bip (1:1,000) (Cell Signaling Technology Cat# 3177, RRID:AB_2119845), anti-CHOP (1:1,000) (Cell Signaling Technology Cat# 2895, RRID:AB_2089254), and anti-GAPDH (1:5,000) (Sigma-Aldrich Cat# G9545, RRID:AB_796208). HRP-conjugated anti-rabbit IgG (1:5,000) (Cell Signaling Technology Cat# 7074, RRID:AB_2099233), and anti-mouse IgG (1:5,000) (Cell Signaling Technology Cat# 7076, RRID:AB_330924) were used as secondary antibodies. The acetylated proteins were visualized by chemiluminescence (GE Healthcare, RPN2235) and detected using a Gel documentation system (BioRad, ChemiDoc™).

Sciatic nerve tissues were washed with ice-cold PBS and lysed in RIPA buffer (Cell Signaling Cat# 9803) containing a cocktail of protease inhibitors (Roche 04693132001) and phosphatase inhibitors (Roche 04906837001) for 30 min on ice. After centrifugation at 15900× *g* for 20 min at 4°C, equal quantities of protein from the supernatants were separated by SDS-PAGE and transferred onto a nitrocellulose membrane (Invitrogen, iBlot® 2 NC Regular Stacks). The blots were then probed overnight at 4°C with a primary antibody against HDAC6 (1:1,000) (Cell Signaling Technology Cat# 7612, RRID: AB_10889735), acetylated α-tubulin (1:2,000) (Cell Signaling Technology Cat# 5335, RRID:AB_10544694), α-tubulin (1:1,000) (Cell Signaling Technology Cat# 2144, RRID:AB_2210548), HSP70 (1:1,000) (StressMarq Biosciences Cat# SMC-100, RRID:AB_854199), myelin protein zero (MPZ; 1:1,000) (Abcam Cat# ab31851, RRID: AB_2144668), human peripheral myelin protein 22 (hPMP22; 1:1,000) (Abcam Cat# ab15506, RRID:AB_301915), myelin basic protein (MBP; 1:1,000) (Abcam Cat# ab40390, RRID:AB_1141521), acetyl-HSP90α K294 (1:1,000) (Rockland Cat# 600-401-981, RRID: AB_2121074), HSP90 (1:1,000) (Cell Signaling Technology Cat# 4877, RRID:AB_2233307), and β-actin (1:1,000) (Sigma-Aldrich Cat# A5441, RRID:AB_476744), followed by the corresponding secondary antibodies. The blots were washed and developed using enhanced chemiluminescence reagents (GE Healthcare RPN2235) according to the manufacturer's instructions. All the protein expression levels were normalized to the expression of β-actin. Band intensity was measured with ChemiDoc MP (BioRad) and quantified using Image Lab™ 5.0 software (BioRad). The immuno-related procedures used comply with the recommendations made by the *British Journal of Pharmacology*.

2.3 | Preparation of T-MSCs and differentiation into Schwann cells

The tonsil MSC (T-MSC) were derived from patients who received a tonsillectomy. The Institutional Review Boards of Ewha Womans University, Mokdong Hospital (IRB No. ECT-11-53-02) and Sungkyunkwan University, Samsung Medical Center (IBR No. SMC 2013-10-124) approved the experimental procedures used in this study. Informed written consent for T-MSC isolation was obtained from the patients' parents or legal guardians before tonsillectomy. T-MSCs were isolated as previously described (Cho, Kim, Kim, Ryu, & Woo, 2012; Jung et al., 2016; Park et al., 2016, 2018). Because paediatric CMT1A patients are required for T-MSC isolation and that it is time-consuming to enrol paediatric CMT1A patients, it was difficult to estimate how many patients may be enrolled within a given study period. Until the preparation of this manuscript, three subjects were enrolled in this study. Thus, we isolated three different T-MSC lines from three paediatric patients. The excised tonsils were minced and digested in DMEM (Invitrogen, Carlsbad, CA, USA) containing 210 $U \cdot ml^{-1}$ collagenase type I (Invitrogen) and DNase (10 $\mu g \cdot ml^{-1}$; Sigma-Aldrich, St. Louis, MO, USA). After the cells had been passed through a cell strainer (BD Biosciences, San Jose, CA, USA), mononuclear cells were obtained by Ficoll–Paque density gradient centrifugation (GE Healthcare, Chicago, IL, USA). The cells were cultured for 48 h at 37°C in low-glucose DMEM containing 10% FBS (Invitrogen) and 1% penicillin/streptomycin (Sigma-Aldrich) in a humidified chamber containing 5% CO_2 in air. To induce the T-MSCs to differentiate into Schwann cells, $1.5–2 \times 10^5$ $cells \cdot cm^{-2}$ were plated in a plastic dish in DMEM/F-12 (Invitrogen) supplemented with 20 $ng \cdot ml^{-1}$ basic FGF (PeproTech, London, UK), 20 $ng \cdot ml^{-1}$ EGF (PeproTech), and 2% B27 supplement (1:50, Gibco, Life Technologies, Burlington, ON, Canada) at 37°C with 5% CO_2 in humidified air. After 7 days, the cells formed aggregates spontaneously to produce neurospheres that were triturated using a 25-gauge needle and plated in laminin-coated cell culture plates containing DMEM/F12 supplemented with 10% FBS, 14 μM forskolin (Sigma-Aldrich), 5 $ng \cdot ml^{-1}$ PDGF-AA (PeproTech), 10 $ng \cdot ml^{-1}$ bFGF (PeproTech), and 200 $ng \cdot ml^{-1}$ recombinant human neregulin-1 (PeproTech) for 10 days with or without 1 μM CKD-504. After terminal differentiation, PMP22 and LAMP1 were analysed by immunocytochemistry

(N = 3). To evaluate the degree of myelination in cocultures, confluent cultures of T-MSC-SCs were trypsinized and added to laminin-coated 2-well cell culture slides (SPL Lifesciences Inc., Seoul, Korea) 1 day before adding dorsal root ganglia (DRGs). To isolate DRG neurons, pregnant ICR mice were purchased from Korean BioLink Co. (Chungbuk, Korea). Gestational day 12.5–13 embryos were removed, and DRGs were collected. These were washed gently twice with 1 ml of DMEM with 10% FBS, then plated directly onto the slides seeded with T-MSC-SCs. They were then incubated for 4 days in coculture medium: Eagle's basal medium, ITS supplement, 0.2% BSA, 4 $mg{\cdot}ml^{-1}$ D-glucose (all from Sigma-Aldrich), Glutamax (Gibco), 50 $ng{\cdot}ml^{-1}$ nerve growth factor (PeproTech), and antibiotics. Then they were grown in the same medium supplemented with 15% FBS and 50 $mg{\cdot}ml^{-1}$ L-ascorbic acid (Sigma-Aldrich) for an additional 3–4 weeks with or without 1 μM CKD-504 to induce myelination (N = 3) (Jung et al., 2016).

2.4 | Immunocytochemistry

Cells cultured on coverslips were fixed in 4% (v/v) paraformaldehyde (Sigma-Aldrich) for 15 min at room temperature or overnight at 4°C. After rinsing in PBS, the fixed cells were permeabilized and blocked using 2% BSA (Bovogen Biologicals, East Keilor, VIC, Australia) in 0.1% Tween-20/PBS, followed by incubation in the diluted primary antibody for 1 h at room temperature or overnight at 4°C with an anti-PMP22 antibody (PMP22; 1:200) (Abcam Cat# ab126769, RRID:AB_11129961), an anti-MBP antibody (MBP; 1:200) (Millipore Cat# AB9348, RRID:AB_2140366), an anti-human mitochondria antibody (1:400) (Millipore Cat# MAB1273, RRID:AB_94052), an anti-neurofilament heavy polypeptide antibody (NF-H; 1:200) (Santa Cruz Biotechnology Cat# sc-20112, RRID:AB_650104), and an anti-LAMP1 antibody (1:200) (Sigma-Aldrich Cat# L1418, RRID:AB_477157). After washing three times in PBS, the samples were incubated for 1 h at room temperature with secondary antibodies with goat anti-chicken IgY (H + L) Alexa Fluor 488 (Molecular Probes Cat# A-11039, RRID:AB_142924) and goat anti-rabbit IgG (H + L) Alexa Fluor 568 (Molecular Probes Cat# A-11011, RRID:AB_143157). The prepared samples were then mounted using Vectashield mounting medium (Vector Laboratories, Burlingame, CA, USA) and analysed using a fluorescence microscope (Nikon Corp., Tokyo, Japan).

2.5 | Animals

All animal care and experimental procedures complied with and were approved by the Institutional Animal Care and Use Committee of the Laboratory Animal Center at Chong Kun Dang (Korea, Inc., IACUC animal study protocol approval number: S-17-033). Animal studies are reported in compliance with the ARRIVE guidelines (Percie du Sert et al., 2020) and with the recommendations made by the British Journal of Pharmacology (Lilley et al., 2020).

C22 mice [B6; CBACa-Tg (PMP22)C22Clh/H], which harbour seven copies of a human PMP22 transgene (Huxley et al., 1996), were obtained from MRC Harwell (Oxfordshire, UK; IMSR Cat# HAR:784, RRID:IMSR_HAR:784). C22 and wild type (WT) mice were produced by in vitro fertilization using 10-week-old C57BL/6J females (OrientBio, KOREA) and 12-week-old C22 males (Macrogen, RRID:SCR_014454). Animals were provided with a standard diet and water ad libitum and housed in a temperature-controlled (22 ± 2°C) and humidity-controlled (44–56%) environment with a 12 h light–dark cycle. Male C22 or WT littermates were used for experiments when they were three weeks old.

2.6 | Design of animal study

For 3 days before the start of the experiment, behavioural tests were conducted for all animals. Using the results of rotarod, grip strength, and body weight measurement, animals were randomly assigned to four experimental groups such as a distilled water (DW) group and three CKD-504 treatment groups (10, 25, 100 $mg{\cdot}kg^{-1}$) with 10 mice per group. The sample size was determined based on our previous study experience with C22 mice. CKD-504 was completely dissolved in distilled water and administered orally twice a day. In 2 weeks after treatment, behavioural tests were performed, and in 3 weeks, electrophysiologic examination was performed. For the histological assessment and immunostaining, the mice were killed a week after the electrophysiologic examination. For the analysis of myelinated- and HDAC6-related protein expression, the sciatic nerves of five animals in each group were analysed. In the analysis of HSP protein expression, only two WT-DW, four C22-DW, and four C22-504 mice could be tested because of the limited amount of remaining sciatic nerve sample.

2.7 | Behavioural testing

The rotarod test and balance beam test were carried out to evaluate motor coordination and balance. The grip strength test was performed to evaluate the degree of muscle atrophy caused by nerve degeneration from CMT. The behavioural tests were performed 30 min after the administration of the test articles.

2.7.1 | Rotarod test

For the adaptation, all test animals received adaptive training five times a day at 8 rpm for 3 days, and animals that met the criterion of latency (falling between 150 and 180 s) were used for further experiments (about 80% of the animals met that criterion). The latency to fall was measured three times at a fixed speed of 8 rpm

for 3 min. The rotarod test was repeated three times per experiment, and the maximum value of the three measurements was used as the test result (ROTA ROD, LE 8205, Panlab). Each experiment was independently evaluated by two experimenters blinded to the drug treatments.

2.7.2 | Balance beam test

A custom-made bar (width 1.2 cm, height 0.6 cm, length 1.0 m) was fixed at a 9° slope (45 cm height at the starting point and 60 cm height at the arrival point). At the departure point, mice were stimulated by 60 W of light. The arrival point was a dark box to let mice feel relief. Every animal was adapted for 30 min before the evaluation under the same conditions as the experimental conditioning. Mice were placed at the departure point and walked to the arrival point. The transit time and slip counts were measured. Before the test, mice were trained three times a day for 2 days. For the slip count and transit time results in the balance beam test, we present the difference between the tests before and after 2 weeks of drug administration. Each experiment was independently evaluated by two experimenters blinded to the drug treatments.

2.7.3 | Grip strength test

The grip strength test (BIO - GS 3, BIOSEB) used a wire mesh grid to evaluate the function of all four feet. All the experiments were conducted by one experimenter, and a maximum value of five successive measurements was used as the test result. Each measurement was performed more than three times. After letting a mouse catch the wire mesh, the experimenter pulled lightly on the mouse to an inclination of about 15° to provide a weak tension and then measured the maximum tension. The experimenter was blinded to the drug treatments.

2.8 | Electrophysiologic examination

The animals were anaesthetized with 2% isoflurane (USP Terrel, Piramal Critical Care, Inc., Bethlehem, PA, USA) in an oxygen/nitrogen oxide mixture, and the fur from the distal back and hind limbs was completely shaved. The skin was maintained >32°C using an external heating device. Electrophysiological recordings were performed on the sciatic nerve, the largest nerve of the peripheral nervous system, using a Nicolet Viking Quest EMG system (Natus Medical, Inc.). The compound motor action potential (CMAP) amplitudes and motor neuron conduction velocity (MNCV) were measured by an independent experimenter who was blinded to the genotype and treatment group. To measure the MNCV, stimulating cathodes were placed at the sciatic notch and 6 mm distal to the sciatic notch, and recording electrodes were placed on the muscle belly of the tibialis anterior muscle. Additionally, a ground electrode was placed on the animal's back, near the midline. CMAPs were measured at supramaximal stimulation.

2.9 | Histological assessment

Sciatic nerves were biopsied from both WT and C22 mice, and pathological examinations of the specimens were performed using light and electron microscopic analyses. Within 0.5 h of the final treatment, the sciatic nerves were collected and fixed in 2.5% glutaraldehyde solution overnight. The fixed samples were processed conventionally for image analysis; 0.5-μm semi-thin sections were prepared and stained with toluidine blue. Epoxy-embedded semi-thin and ultra-thin sections were prepared for light and ultrastructural examinations (Hong et al., 2016). To visualize the actin and nuclei, the collected nerves were stained with rhodamine conjugated phalloidin (Thermo Fisher Scientific Waltham, MA) and mounted with DAPI containing Vectashield (Vector Laboratories, Burlingame, CA), as previously reported (Jung et al., 2011). Morphometric analyses, such as the diameters of axons (myelinated and unmyelinated fibres) and g-ratio, were performed in ImageJ software (RRID:SCR_003070). The total number of axons in the left sciatic nerve of each animal were counted. The numbers of myelinated axons are expressed as a percentage of the total counted axons. Internodal length was determined by measuring the distance between nuclei stained with DAPI, following the protocol in the previous report (Shin et al., 2014). The sample size of each group was as follows: DW-treated WT: $N = 5$; DW-treated C22: $N = 5$; CKD-504-treated C22: $N = 5$.

2.10 | Immunohistochemistry

For immunohistochemical testing, the sciatic nerve tissues were fixed in 10% formalin. The paraffin block was sectioned at 3 μm, and then deparaffinization, antigen retrieval, permeabilization, and blocking for immunofluorescent staining were performed. PMP22 primary antibody (Abcam, Cat. No. ab15506) was diluted to 1:200 and incubated for reaction at room temperature for 90 min. Secondary antibody Alexa Fluor 594 goat anti-rabbit IgG (ThermoFisher Scientific, Cat. No. A11012) was diluted to 1:1,000 and reacted overnight at 4°C. Anti mono- and polyubiquitin conjugate monoclonal antibody (Enzo, Cat. No. BML-PW8810) for ubiquitin detection was diluted to 1:200 and reacted for 90 min. Then, secondary antibody Alexa Fluor 488 goat anti-mouse IgG (ThermoFisher Scientific, Cat. No. A32723) was diluted to 1:1,000, added, and left overnight at 4°C. Slides were then exposed to DAPI (ThermoFisher Scientific, Cat. No. D1306) for nuclear counterstaining and mounted. Cell counts were conducted using a 400× objective fluorescent microscope. We designated ten 100 μm X 100 μm regions of interest (ROIs) from stable areas. Each average number of PMP22 aggregates, ubiquitinylated protein

aggregates, merged aggregates of PMP22, and ubiquitinylated proteins and nuclei was obtained from five different ROIs. To exclude background staining, measurements were conducted using the colour counter function of ImageJ software (RRID: SCR_003070), and the red, green, and yellow minimum thresholds were set to 80 to confirm the aggregates detected after modification. Nuclei were counted from every area of the picture. Every measurement was conducted using the same standard, and the experimenters were blinded to the drug treatments. The sample size of each group was as follows: DW-treated WT: $N = 5$; DW-treated C22: N = 5; CKD-504-treated C22: $N = 5$.

2.11 | Data and statistical analysis

The data and statistical analysis comply with the recommendations of the *British Journal of Pharmacology* on experimental design and analysis in pharmacology (Curtis et al., 2018). Images of western blots were quantified using Image Lab 5.0 (Bio-Rad Laboratories 2013). All immunohistochemistry, semi-thin, and ultrastructure images were quantified using ImageJ software (RRID:SCR_003070). All experiments were designed to generate groups using randomization and blinded analysis. Data are presented as the mean ± SEM, and each analysis was repeated to confirm reproducibility. One-way ANOVA was performed to compare three groups or more. When F in the ANOVA results achieved the necessary level of statistical significance, and there was no significant variance inhomogeneity, post hoc tests were conducted using Dunnett's test. Differences were considered to be statistically significant when $P < 0.05$. All the statistical analyses were performed using GraphPad Prism 5.0 (RRID: SCR_002798).

2.12 | Materials

Forskolin was obtained from Sigma-Aldrich, PDGF-AA, bFGF, and recombinant human neregulin-1 were obtained from PeproTech. CKD-504 is a new inhibitor of HDAC6 developed by the Chong Kun Dang Pharmaceutical Corporation (CKD Pharm, Korea). CKD-504 is a potent and highly selective hydroxamic acid HDAC6 inhibitor. An international patent was registered in 2015 (WO2015137750A1). Its MW is about 390 $g \cdot mol^{-1}$, and its solubility is more than 100 $mg \cdot ml^{-1}$ in water (highly water-soluble compound). It is a hydroxybenzamide class HDAC6 inhibitor (Figure S1). **LBH-589 (panobinostat)**, a pan HDAC inhibitor, was purchased from LC Labs, USA (P-3703). For the in vitro enzyme assay and α-tubulin acetylation assay, these chemicals were dissolved in DMSO (Sigma-Aldrich, St. Louis, MO, USA). The stock solutions were kept at −20°C and diluted to the required concentrations in growth medium as needed. Vehicle (DMSO) was used in the negative control groups. The final concentration of DMSO was less than 0.1%.

2.12.1 | Nomenclature of targets and ligands

Key protein targets and ligands in this article are hyperlinked to corresponding entries in the IUPHAR/BPS Guide to PHARMACOLOGY (http://www.guidetopharmacology.org) (Harding et al., 2018) and are permanently archived in the Concise Guide to PHARMACOLOGY 2019/20 (Alexander, Fabbro et al., 2019; Alexander, Kelly et al., 2019).

3 | RESULTS

3.1 | A novel, selective HDAC6 inhibitor with competitive binding for HDAC6 enzyme

CKD-504 is a potent and highly selective hydroxamate HDAC6 inhibitor that chelates Zn^{2+} ions in the catalytic domain of HDAC6. In the HDAC panel assay, CKD-504 selectively inhibited HDAC6, with the IC_{50} of 46 ± 8.5 nM. The IC_{50} on HDAC8 was 6.6 ± 1.3 μM. The IC_{50} values on the other HDAC isoforms were above 10 μM, indicating excellent enzyme selectivity (Figure 1a). To confirm the intracellular potency and selectivity of CKD-504, its effect on the acetylation of α-tubulin, a major HDAC6 target protein, and histone H4 was analysed in human PBMCs (Figure 1b). CKD-504 exhibited dose-dependent (from 30 nM) inhibition of HDAC6, in terms of the acetylation of α-tubulin, without affecting the acetylation of histone H4, which is a representative nuclear target protein of other class I HDAC isoforms. In the kinetics study, CKD-504 was predicted to be a competitive inhibitor against HDAC6, with K_i of 6.28 nM and residence time of 61.3 min (Figure 1c–e). These results confirm that CKD-504 is a potent and selective HDAC6 inhibitor with a competitive binding mode for the HDAC6 enzyme.

3.2 | T-MSC-derived Schwann cells treated with CKD-504 has less PMP22 proteins and more myelination in a neuron-Schwann cell coculture system

The therapeutic potential of HDAC6 inhibition has been well established in CMT2F caused by the defective axonal transport. HDAC6 inhibition has been reported to enhance axonal transport and, thus, improve neuronal function (Adalbert et al., 2020; Benoy et al., 2017, 2018; d'Ydewalle et al., 2011; Mo et al., 2018). However, the therapeutic potential of HDAC6 inhibition has not yet been tested in CMT1A caused by the defective myelination of Schwann cells. To test the therapeutic potential of CKD-504 in CMT1A, we analysed its effect on PMP22 expression in Schwann cells derived from the T-MSCs of healthy donors or CMT1A patients, as previously described (Figure 2a) (Jung et al., 2016). These exploratory results are derived from a small group of patients

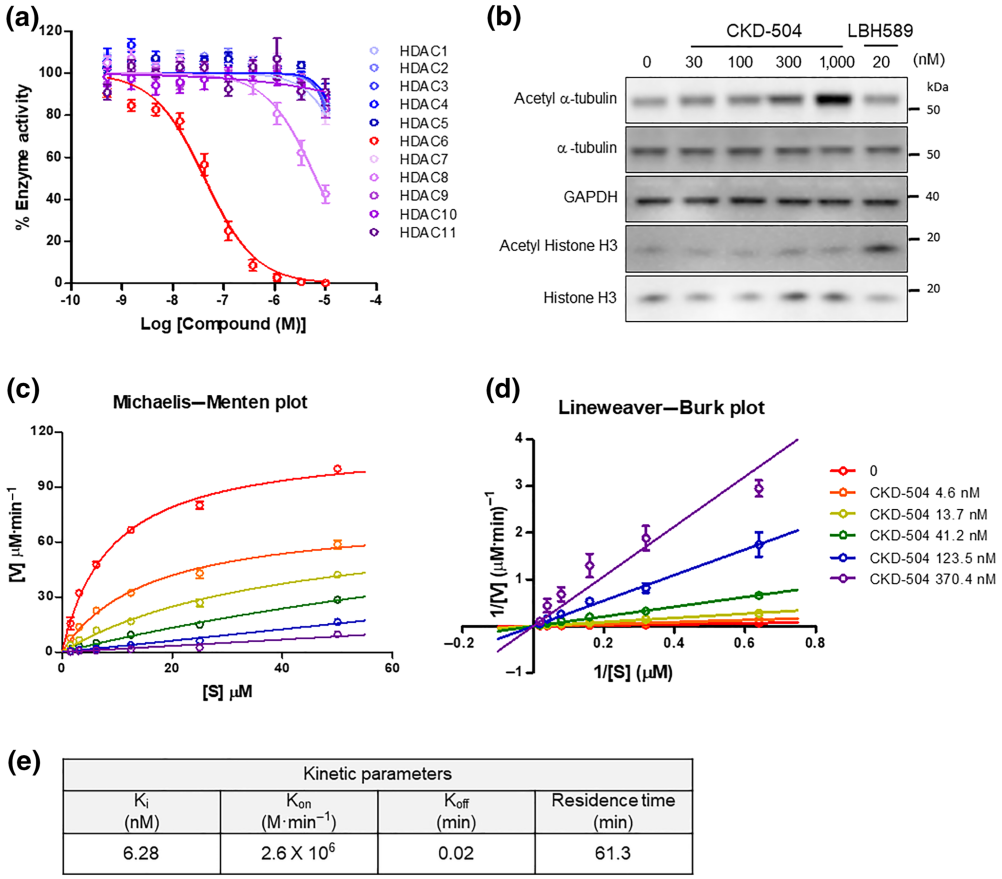

(e)

Kinetic parameters			
K_i (nM)	K_{on} ($M \cdot min^{-1}$)	K_{off} (min)	Residence time (min)
6.28	2.6×10^6	0.02	61.3

FIGURE 1 A novel, potent, and selective HDAC6 inhibitor, CKD-504. (a) The inhibitory effects of CKD-504 on the enzymatic activity of 11 HDACs. The *y*-axis represents the percentage of basal enzymatic activity corresponding to various concentrations of CKD-504. Curve-fitting of a 10-point enzymatic assay starting from 10 μM with threefold serial dilution (Reaction Biology Corp, Malvern, PA). This result was repeated five times. (b) The effects of CKD-504 on the acetylation of α-tubulin, an HDAC6 substrate, in human PBMCs. Acetylated histone H3 was used as a control for enzyme selectivity. The western blot analysis result is a representative one of five independent experiments. LBH-589 (PARYDAK®, Novartis) is a pan-HDAC inhibitor developed as an anticancer agent. The kinetic study of CKD-504 was performed with HDAC6 enzyme. CKD-504 and a fluorogenic substrate (RHKK-Ac-AMC) were diluted to appropriate concentrations, and then the enzyme reaction was performed as described in the methods. (c) The Michaelis–Menten plot and (d) the Lineweaver–Burk plot are presented. (e) The kinetic parameters (K_i, K_{on}, K_{off}, and residence time) of CKD-504 were calculated. The data are presented the average values from five independent experiments. Data were presented as mean ± SEM. One-way ANOVA was performed for comparison among groups. It was considered that the difference was statistically significant if $P < 0.05$

($N = 3$). Compared with T-MSC-derived Schwann cells (T-MSC-SCs) from a healthy donor, the T-MSC-derived Schwann cells from CMT1A patients (CMT1-SCs) expressed more PMP22 protein, which formed speckle-like protein aggregates, as described previously (Figure 2b) (Jung et al., 2016). The CMT1-SCs treated with CKD-504 (1 μM) for 10 days (Schwann cell differentiation stage) expressed less PMP22, about 14% of the amounts in control, untreated CMT1-SCs and had fewer PMP22 protein aggregates (Figure 2b,c). Although LAMP1, a lysosome marker, was weakly distributed in CMT1-SC cytosol, CMT1-SCs treated with CKD-504 had more LAMP1 protein by 2.9-fold, suggesting that CKD-504 might enhance lysosome-mediated protein degradation (Figure 2b, d). In addition, the formation of myelin sheaths was analysed by double staining with anti-MBP and anti-NF-H antibodies. The myelination ratio was calculated by dividing the number of myelinated axons by the number of total axons. The myelination ratio of CMT1-SCs with the DRG-derived axons were 85% lower than the ratio with T-MSC-SCs (Figure 2e,f). The myelination ratio of CMT1-SCs co-cultured with DRG neurons exhibited more myelination, by 4.2-fold, after CKD-504 (Figure 2e,f). The myelination of the DRG-derived axons was induced by SCs differentiated from human-origin MSCs, which was confirmed by double staining with anti-MBP and anti-human mitochondria antibodies (Figure S2).

3.3 | CKD-504 improved behaviour, balance, and electrophysiological findings in C22 mice

To evaluate the efficacy of CKD-504, C22 mice were treated with CKD-504 orally twice a day for 3 weeks. To evaluate their behaviour and sensorineural functional recovery, rotarod, grip

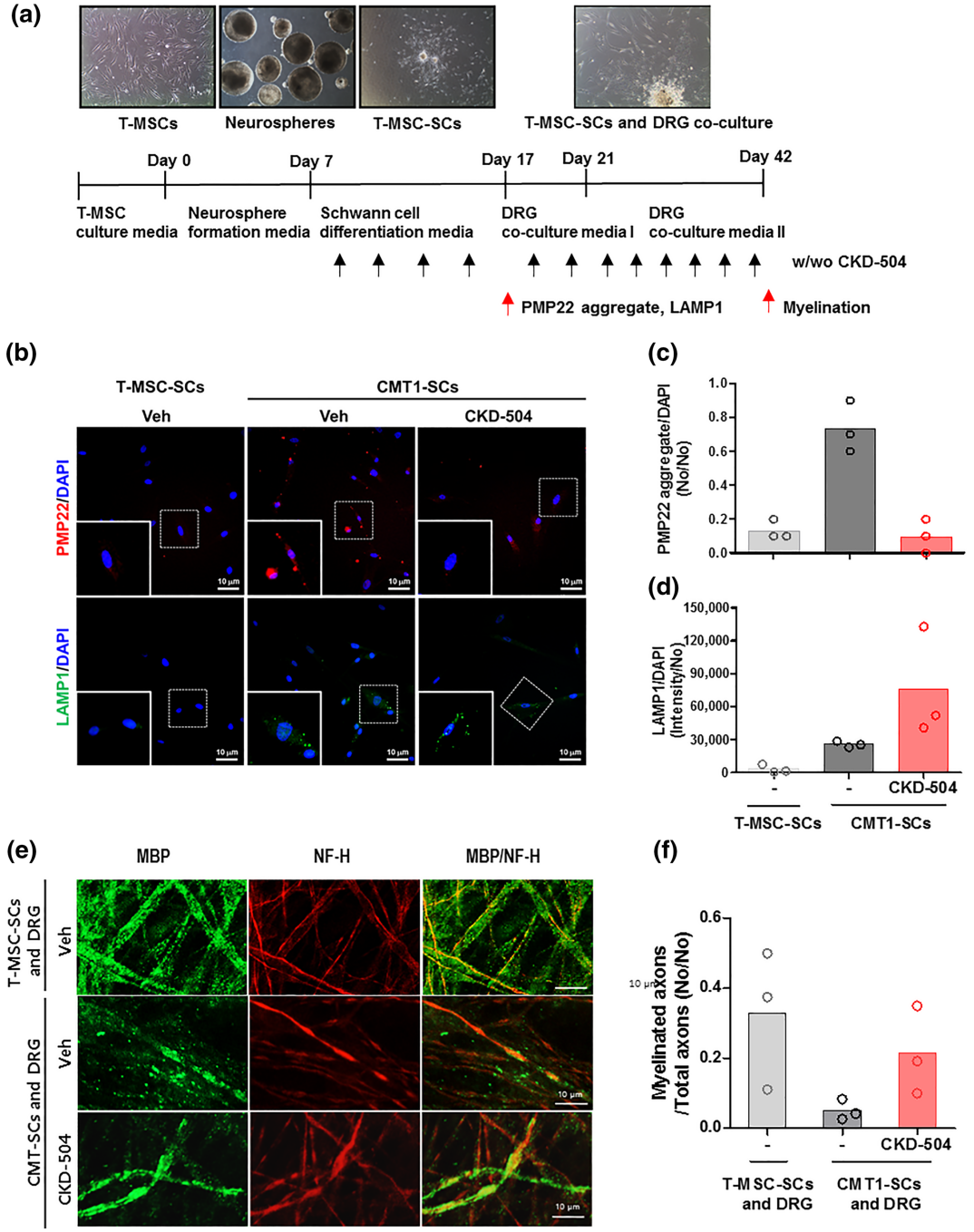

FIGURE 2 CMT1-TMSC-SC treated with HDAC6 inhibitor had less PMP22 aggregation and more myelination when cocultured with DRG neurons. (a) Experiment scheme for Schwann cell differentiation from human tonsil-derived mesenchymal stem cells (T-MSCs) and for the induction of myelination using T-MSC-SCs cocultured with DRG neurons. (b) Representative immunocytochemical staining for PMP22 aggregates (red), LAMP1 (green), and DAPI (blue). (c, d) PMP22 aggregates and LAMP1 were normalized with DAPI and presented as a scatterplot with mean; *N* = 3 per group. (e) Representative immunocytochemical staining of NF-H (red) and MBP (green) indicate the formation of myelin sheaths by CMT1-SCs; 200×, scale bar = 10 μm. (f) Myelination ratio of DRG-derived axons with T-MSC-SCs and CMT1-SCs with or without CKD504 treatment were presented as a scatterplot with mean; *N* = 3 per group. CMT1-SCs, Schwann cells derived from T-MSC of CMT1A paediatric patients; T-MSC, tonsil-derived mesenchymal stem cell; T-MSC-SC, Schwann cells derived from T-MSC of healthy donors

strength, and balance beam tests were performed after 2 weeks of treatment. A week after that, nerve conduction was analysed, and then the mice were killed for further histological analyses (Figure 3a). CKD-504 treatment for 3 weeks did not affect the body weight of C22 mice (Figure S3).

To confirm that oral treatment with CKD-504 inhibited HDAC6 in the sciatic nerve, we analysed the acetylation of α-tubulin. The sciatic nerve and DRGs of C22 mice treated with CKD-504 exhibited more acetylation of α-tubulin, suggesting that CKD-504 is well delivered to both the sciatic nerve and DRGs (Figure S4).

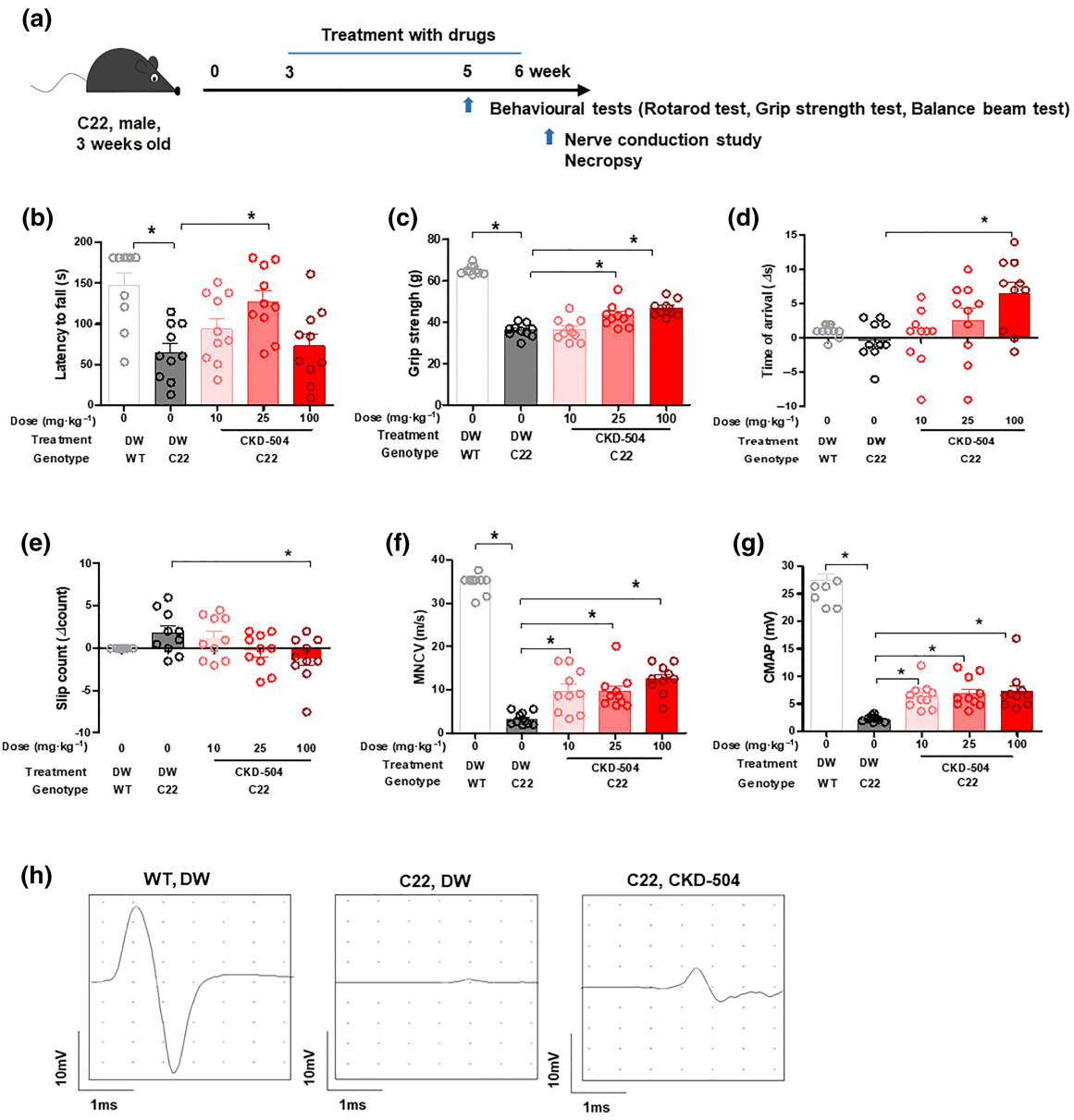

FIGURE 3 Improvement in the behavioural and electrophysiological phenotypes of C22 mice after treatment with HDAC6 inhibitor. Three-week-old C22 mice were orally treated twice a day with DW or CKD-504 (10, 25, and 100 mg·kg^{-1}) for 3 weeks; $N = 10$ per group. WT littermates treated with DW were included as controls. (a) Animal experiment scheme. (b) Latency to fall on rotarod test, (c) grip strength, (d) transit time, and (e) slip count on the balance beam were measured after 2 weeks of treatment. (f) MNCV and (g) CMAP were measured after 3 weeks of treatment. (h) Representative electrophysiological graphs are presented (CKD-504: 25 mg·kg^{-1}). Data were presented as mean ± SEM. One-way ANOVA was performed for comparison among groups. It was considered that the difference was statistically significant if $P < 0.05$

The locomotor behaviour of the treated mice was analysed by a rotarod test, and we found that C22 mice treated with 25 mg·kg^{-1} of CKD-504 remained on the rod longer than control C22 mice (Figure 3b). In the double normalization result, the CKD-504 group showed an improvement of 75% ([%improvement] = ([CKD-504] – [C22])/([WT] – [C22]). In the grip strength test, CKD-504 treatment exhibited significant improvement from 25 mg·kg^{-1} (Figure 3c). In the balance beam test, to evaluate sensorineural balance and coordination, CKD-504 significantly improved the transit time (Figure 3d) and slip count (Figure 3e), in a dose-dependent manner. These findings demonstrate that motor function and sensory-motor balance were efficiently improved by CKD-504.

We also used an electrophysiological analysis to determine whether CKD-504 treatment improved function. In C22 mice, we found significantly increased motor nerve conduction velocity in a

dose-dependent manner (Figure 3f,h). Moreover, the CKD-504-treated mice showed a significant increase in the amplitude of the compound muscle action potential (Figure 3g,h). Taken together, these data imply that CKD-504 has significant therapeutic efficacy in this model of CMT1A.

3.4 | CKD-504 restored the myelination and morphology of the sciatic nerve in C22 mice

To further evaluate the efficacy of CKD-504 in improving peripheral nerve function, we analysed the myelination and axon diameter in semi-thin cross-sections from sciatic nerves. Demyelinated axons and onion bulb formations are the pathological hallmarks of CMT1A. C22 mice had more thinly myelinated or non-myelinated axons in the sciatic nerve than WT mice did. The sciatic nerves of CKD-504-treated C22 mice had a thicker myelin structure than those of DW-treated C22 mice, and we found that CKD-504 treatment partly rescued the histopathological phenotypes of C22 mice (Figure 4a,b). When we measured the number of axons that were myelinated, unmyelinated, or exhibiting onion bulb formation, we found a significant increase in myelinated axons and a reduction in unmyelinated axons and those showing onion bulbs in C22 mice that had received 3 weeks of CKD-504 treatment compared with DW-treated C22 mice (Figure 4c–f). More abundant myelinated axons and larger

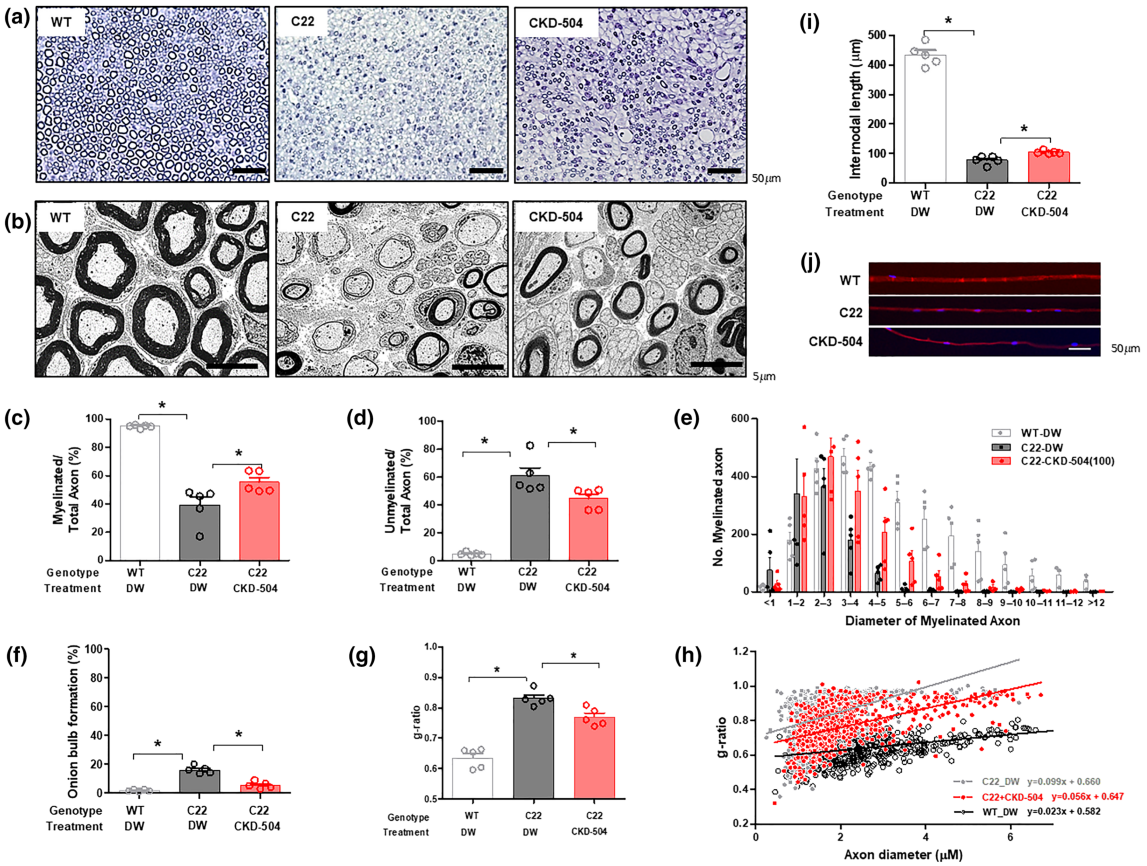

FIGURE 4 Histopathological improvement in C22 mice after HDAC6 inhibitor treatment. Three-week-old mice were orally treated twice a day with DW or 100 mg·kg^{-1} CKD-504 for 3 weeks; *N* = 5 per group. WT littermates treated with DW were included as controls. (a, b) Representative semi-thin (200×, scale bar: 50 μm) and ultrastructure images (4,000×, scale bar: 5 μm) of toluidine blue-stained sciatic nerve cross-sections were presented. The diameters of the myelinated or unmyelinated axons were measured for the indicated treatment groups. (c) Ratio of myelinated axons and (d) unmyelinated axons to the total number of axons. (e) The diameters of myelinated axons were plotted as a histogram to show their size distribution. (f) The percentage of onion bulb axons was quantified. (g) The average g-ratio in each group was analysed. (h) A scatterplot exhibited the relationship between the g-ratio and axonal diameter (WT-DW: *n* = 642; C22-DW: *n* = 744; C22–504: *n* = 680). (i) Internodal length (200×, scale bar: 50 μm) was determined by measuring the distance between nuclei (WT-DW: *n* = 87; C22-DW: *n* = 422; C22-504: *n* = 396). (j) Representative images of internodal length were presented (200×, scale bar: 50 μm). WT-DW, wild type mice treated with distilled water; C22-DW, C22 mice treated with distilled water; C22-CKD-504 (100), C22 mice treated with 100 mg·kg^{-1} of CKD-504. Data were presented as mean ± SEM. One-way ANOVA was performed for comparison among groups. It was considered that the difference was statistically significant if $P < 0.05$

myelinated axons were also observed in the C22 mice treated with CKD-504 than in the control C22 mice treated with DW (Figures 4e and S5). As a quantitative analysis, we evaluated the g-ratio by measuring the inner and outer diameters of the axons. The g-ratios of CKD-504-treated C22 mice had a lower slope than those of the DW-treated C22 mice. The average g-ratios were 0.64 ± 0.01 (DW-treated WT mice), 0.83 ± 0.01 (DW-treated C22 mice), and 0.77 ± 0.01 (CKD-504-treated C22 mice) (Figure 4g,h). In the analysis of teased sciatic nerve, the average internodal lengths were 433 ± 16.1 μm (DW-treated WT mice), 77.8 ± 6.4 μm (DW-treated C22 mice), and 104 ± 2.3 μm (CKD-504-treated C22 mice), indicating that the CKD-504-treated C22 mice had significantly longer internodal lengths than the DW-treated C22 mice (Figure 4i,j).

3.5 | CKD-504 reduced PMP22 protein aggregation without affecting overall ubiquitinated proteins in the sciatic nerves of C22 mice

Protein aggregates often indicate reduced ubiquitin-proteasomal activity, which causes an accumulation of ubiquitinated proteins (Bence, Sampat, & Kopito, 2001; Johnston, Ward, & Kopito, 1998). In C22 mice, an accumulation of ubiquitinated PMP22 aggregates was observed, and it was previously reported that the accumulation of ubiquitinated PMP22 protein was caused by defective proteasomal activity (Fortun et al., 2006, 2007).

In our in vitro Schwann cell analysis, CKD-504 reduced the number of PMP22 protein aggregates by enhancing lysosomal activity. To analyse the effect of CKD-504 treatment on PMP22

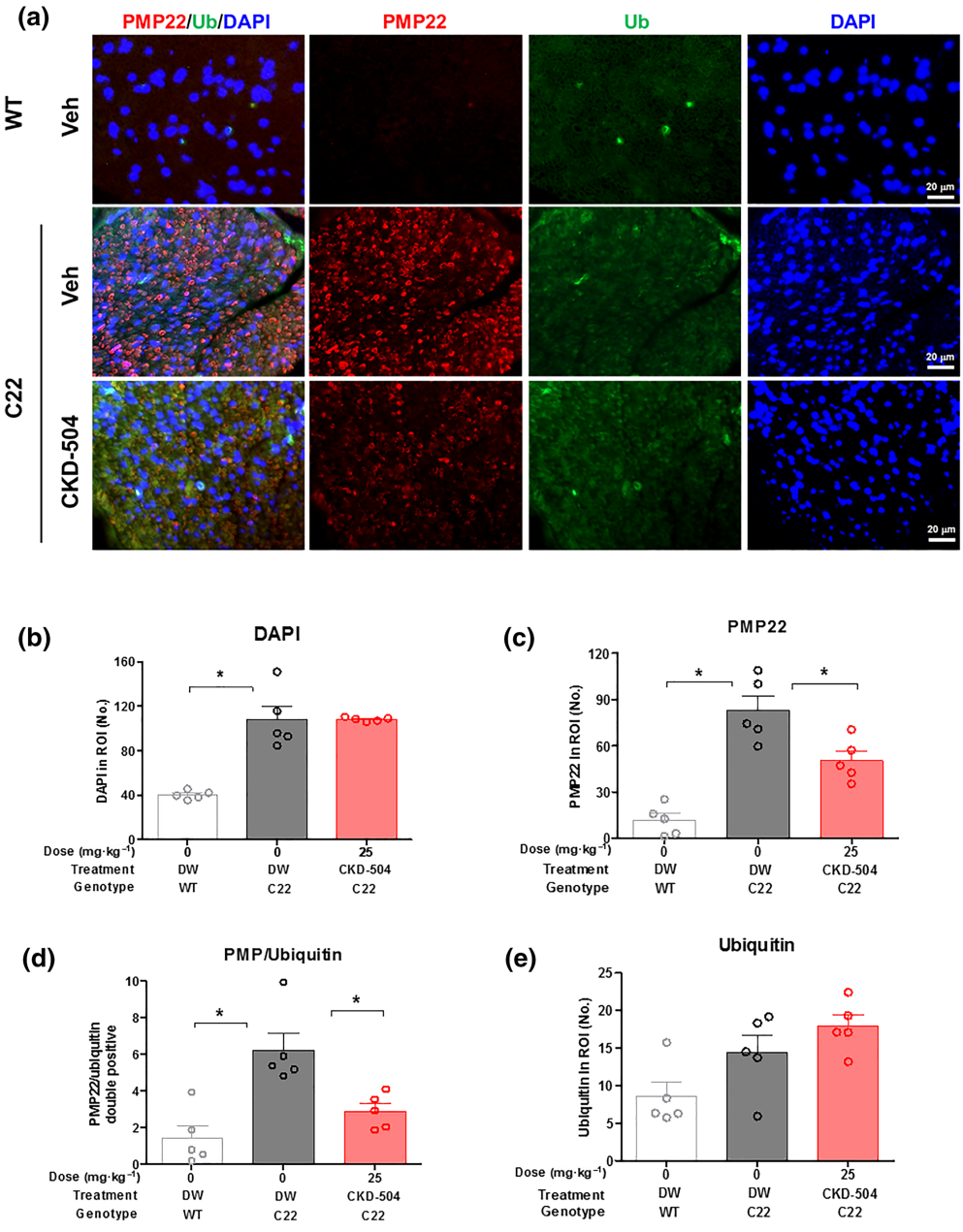

FIGURE 5 HDAC6 inhibitor reduced the number of ubiquitinated PMP22 aggregates in the sciatic nerves of C22 mice. Three-week-old mice were orally treated twice a day with DW (N = 7) or CKD-504 (100 mg·kg^{-1}) for 3 weeks (N = 8). WT littermates treated with DW were included as controls (N = 6). (a) Immunohistochemical staining for PMP22 aggregates (red), ubiquitinated protein (green), merged images (orange), and nuclei (blue). The percentages of (b) DAPI, (c) PMP22 aggregate, (d) PMP22 aggregate/ubiquitin double positive speckle, and (e) ubiquitin speckle were presented. C22 mice had more PMP22 aggregates and ubiquitinated speckles than WT mice. CKD-504 reduced the number of PMP22 aggregates but did not affect that of ubiquitin speckles. Scale bar: 20 μm (400×). Data were presented as mean ± SEM. One-way ANOVA was performed for comparison among groups. It was considered that the difference was statistically significant if $P < 0.05$

protein expression or aggregation in the sciatic nerves of C22 mice, we performed an immunofluorescence analysis (Figure 5a). Hypercellularity of Schwann cells was observed in C22 mice compared with WT mice, due to the axonal degeneration and was not changed by CKD-504 treatment (Figure 5a,b). CKD-504 reduced PMP22 protein expression in the sciatic nerve by 45% compared with sciatic nerve sections from DW-treated C22 mice (Figure 5c). The PMP22 colocalized with ubiquitin was equivalent to PMP22 aggregate reduction (Figure 5d). However, the total number of ubiquitinated protein aggregates was similar even after CKD-504 treatment for 3 weeks (Figure 5e), suggesting that CKD-504 reduced PMP22 expression through a pathway other than the ubiquitin-proteasome pathway.

3.6 | C22 mice treated with CKD-504 had more acetylation of HSP90 and expression of HSP70, a key protein in the unfolded protein response

Misfolded PMP22 protein can be refolded by chaperone proteins in the endoplasmic reticulum. If refolding PMP22 is not possible, the proteins are translocated back to the cytoplasm and cleared by the ubiquitin-proteasome pathway (Ryan, Shooter, & Notterpek, 2002). In C22 mice, proteasome activity is so weak that PMP22 aggregates are widely distributed (Fortun et al., 2006). It has been reported that inducing chaperone proteins, such as HSP, can reduce the formation of PMP22 aggregates (Fortun et al., 2007), suggesting that an increase in the folding/refolding process could help inhibit the formation of new PMP22 aggregates and thereby reduce the number of ubiquitinated PMP22 protein aggregates. In particular, the acetylation of HSP90 was reported to induce the expression of HSP70 and other chaperone proteins, leading to a reduction in PMP22 aggregate formation (Kovacs et al., 2005).

In the immunofluorescence analysis, CKD-504 reduced the formation of PMP22 aggregates without affecting the ubiquitinated protein level (Figure 5c,e), suggesting that the reduction of PMP22 aggregates by CKD-504 could be due to increased folding/refolding by chaperone proteins instead of the proteasome pathway. CKD-504 treatment induced the acetylation of α-tubulin in the sciatic nerve, indicating that CKD-504 was well distributed in the sciatic nerve (Figure 6a). C22 mice treated with CKD-504 exhibited higher acetylation of HSP90 than C22 treated with DW, by 70%. In line with the previous reports that the acetylation of HSP90 induces the expression of HSP70 protein (Bali et al., 2005), CKD-504 induced the expression of HSP70 protein significantly in the sciatic nerve of C22 mice (Figures 6a–e and S6). Taken together, these results strongly suggest that CKD-504 reduced the number of PMP22 aggregates by modulating chaperone activity, which resulted in remyelination of peripheral nerve axons and improvement of motor function and electrophysiological parameters.

4 | DISCUSSION

In this study, CKD-504, a novel, selective HDAC6 inhibitor at the clinical development stage, reduced PMP22 protein expression and induced Schwann cell differentiation in an in vitro coculture system. CKD-504 induced the acetylation of α-tubulin in the sciatic nerve of C22 mice, implying that CKD-504 was well-distributed in the sciatic nerve, where the higher acetylation of HSP90 and the expression of HSP70 were observed. CKD-504 reduced the amount of PMP22 protein in the sciatic nerves of C22 mice. As a result, CKD-504 restored myelination of the sciatic nerve and improved the electrophysiological parameters and motor functions of C22 mice. Taken together, these results suggest that this novel HDAC6 inhibitor, CKD-504, could become a new therapeutic option for CMT1A patients.

HDAC6 is an attractive drug target for neurodegenerative diseases, as shown by the accumulating evidence for the therapeutic efficacy of its inhibition. In addition, HDAC6 is a safe target for inhibition because HDAC6 knockout mice are viable and fertile with a normal lifespan (Seidel et al., 2015; Zhang et al., 2008).

4.1 | Pleiotropic function of HDAC6

HDAC6 is involved in various stress responses, such as microtubule dynamics (Zilberman et al., 2009), the unfolded protein response, autophagy (Pandey et al., 2007), the production of NADPH oxidase-induced ROS (Youn, Cho, Kim, Choi, & Park, 2017), and fibrosis by TGFβ signalling (Shan et al., 2008; Tao, Yang, Hu, Shi, & Li, 2016; Xu et al., 2017). In addition, HDAC6 controls the interaction between microtubule and motor proteins (such as kinesin and dynein) and axonal transport (Helleputte, Benoy, & Bosch, 2014). In the immune system, HDAC6 is involved in the vicious cycle of inflammatory response driven by NADPH oxidase: NADPH oxidase generates ROS, which induces an extensive inflammatory response. In this process, HDAC6 collaborates with NADPH oxidase to strengthen the inflammatory response by inducing cytokines, chemokines, and cell adhesion molecules (Youn et al., 2017).

4.2 | HDAC6 in axonal transport

Interestingly, HDAD6 has been reported to modulate the transport and fusion-fission cycle of mitochondria, which is one of key organelles controlling oxidative stress in cells (Guedes-Dias et al., 2015). The fusion-fission cycle and transport of mitochondria depend on microtubule stability and dynamics. HDAC6 removes the acetyl group from the ε-amino group of α-tubulin Lys40, which reduces microtubule stability or dynamics (Skultetyova et al., 2017). Given that the rapid axonal transport of intracellular vesicles and mitochondria is involved in many neurological disorders, including CMT2F, it is reasonable to consider HDAC6 as a

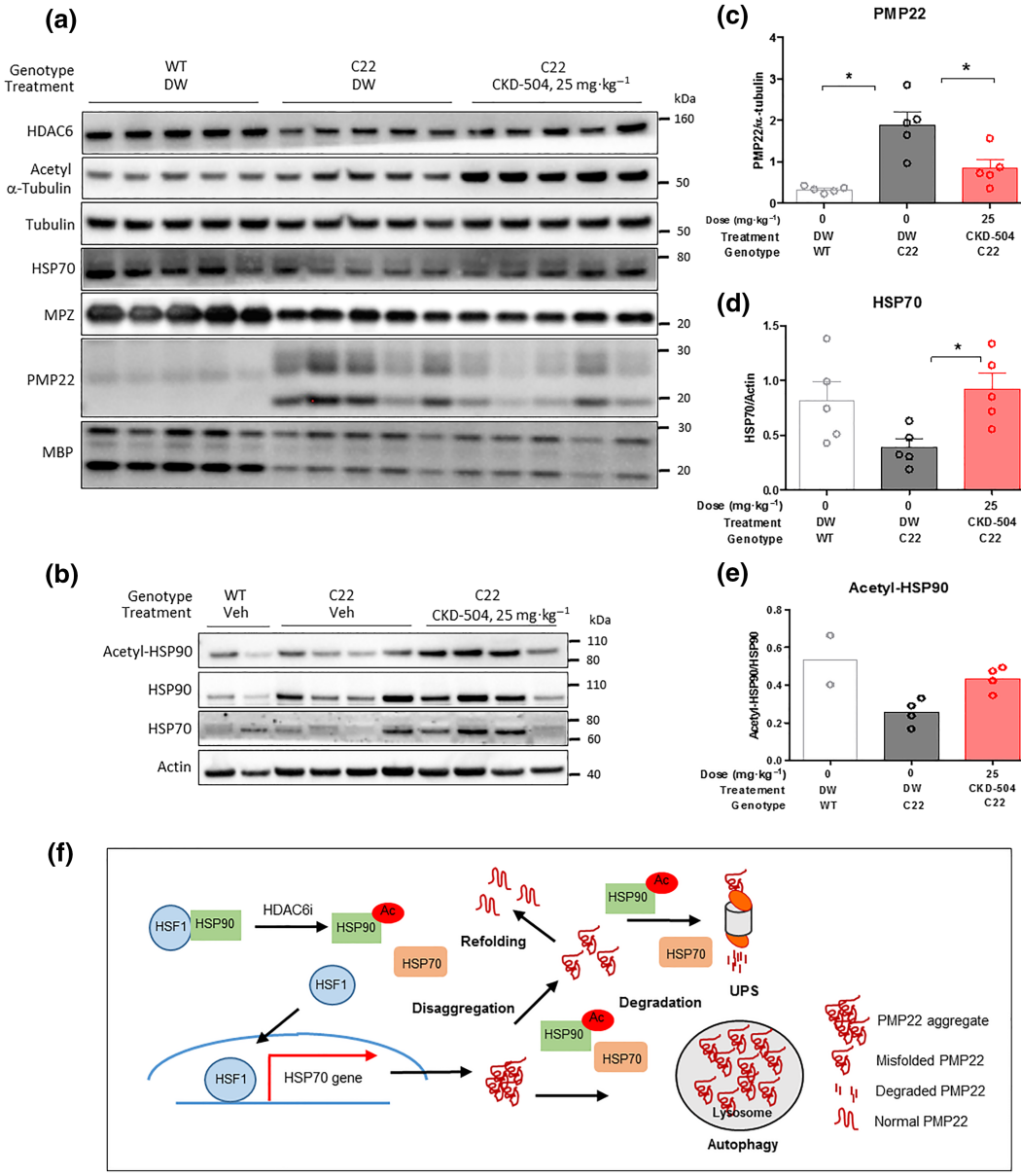

FIGURE 6 HDAC6 inhibitor reduced PMP22 expression by modulating molecular chaperone proteins such as HSP90 and HSP70. For the analysis of protein expression, CKD-504 was administered twice a day for 3 weeks, and the sciatic nerves were collected within 0.5 h after the last treatment. (a) Myelination- and HDAC6-related protein expression were analysed (WT-DW: *N* = 5; C22-DW: *N* = 5; C22-504: *N* = 5). (b) The acetylation of HSP90 and expression of HSP70 were analysed (WT-DW: *N* = 2; C22-DW: *N* = 4; C22-504: *N* = 4). (c) PMP22, (d) HSP70, and (e) acetylated HSP90 expression were measured. (f) The proposed model for the therapeutic mechanism of CKD-504 in CMT1A mice. Data were presented as mean ± SEM. One-way ANOVA analysis was performed for comparison among groups. It was considered that the difference was statistically significant if $P < 0.05$

promising therapeutic target for neurodegenerative diseases (d'Ydewalle et al., 2011; Kneynsberg, Combs, Christensen, Morfini, & Kanaan, 2017; Millecamps & Julien, 2013; Simoes-Pires et al., 2013).

We previously reported that the axonal transport deficit in motor neurons differentiated from induced pluripotent stem cells derived from patients with a heat shock protein β-1 mutation could be rescued by inhibiting HDAC6 to increase the acetylation of α-tubulin (Kim et al., 2016). In a CMT2F animal model of defective axonal transport due to reduced microtubule stability, inhibition of HDAC6 restored the acetylation of α-tubulin and axonal transport, rescuing peripheral nerve function in CMT2F animals (d'Ydewalle et al., 2011). Interestingly, CKD-504 also improved mitochondrial transport along the axons of cultured C22 mouse peripheral nerve cells (Figure S7, Videos S1–S3).

4.3 | PMP22 protein aggregates in CMT1A

PMP22 is a 22-kDa multi-spanning membrane protein that requires a complex folding process and is mainly expressed in Schwann cells.

PMP22 interacts with an actin cytoskeleton to induce the myelination of Schwann cells (Lee et al., 2014). About 80% of newly synthesized PMP22 degrades rapidly due to inefficient folding, suggesting that its tight regulation might be important in proper Schwann cell differentiation. Interestingly, both point-mutations and the overexpression of PMP22 have been reported in CMT1A patients, though the point-mutation shows a wider spectrum and more severe phenotypes than gene duplication (Scherer & Chance, 1995). In addition, PMP22 protein aggregation in the cytoplasm is observed more clearly in patients with a point-mutation than in patients with gene duplication (Hanemann, D'Urso, Gabreëls-Festen, & Müller, 2000). Those results suggest that PMP22 protein overexpression could induce CMT1A and that PMP22 protein aggregates, in addition to protein overexpression, might exacerbate the pathogenesis of CMT1A. The overexpression of PMP22 induces the unfolded protein response, along with a significant accumulation of PMP22 aggregates in CMT1A patient samples and the Schwann cells of CMT1A model animals (Fortun et al., 2006; Lee et al., 2018; Notterpek, Ryan, Tobler, & Shooter, 1999).

4.4 | HDAC6 in unfolded protein response

HDAC6 is involved in the unfolded protein response (UPR) process for handling misfolded proteins in cells, in addition to its function in controlling microtubule stability and protein transport (Ouyang et al., 2012; Yan et al., 2013). HDAC6 might also control protein activity by forming protein complexes to modulate the subcellular localization or activity of target proteins such as glucocorticoid receptors and mineralocorticoid receptors (Jimenez-Canino et al., 2016; Rimando et al., 2016). Furthermore, HDAC6 induces the acetylation of HSP90, which interacts with various cytosolic client proteins in a well-established HSP90 chaperone network and induces other chaperone proteins necessary for protein refolding (Zhao & Houry, 2005).

In T cells, HDAC6 is required for proper T cell receptor (TCR) signalling, where it stabilizes the lymphocyte-specific protein tyrosine kinase, a key signal transducer of the TCR complex, probably by controlling the molecular chaperone system in T cells (Tsuji, Okiyama, Villarroel, & Katz, 2015). HSP90, a downstream protein of HSP70, binds to its client proteins to offer more surface area with hydrophobic and hydrophilic residues for the formation of the protein core and allows its client proteins to reach normal folding status without interference by chaperones (Saibil, 2013). The acetylation of HSP90 is an important posttranslational modification to control its chaperone function, resulting in the induction of other chaperone proteins to compensate for the reduced chaperone activity of HSP90. The inactivation of HDAC6 induces the acetylation of HSP90 at Lys294, dissociation from its co-chaperone protein, p23, loss of chaperone function, and the depletion of several HSP90 client proteins (Bali et al., 2005; Fiskus et al., 2007; Kovacs et al., 2005; Scroggins et al., 2007). According to the previous studies, the acetylation of HSP90 reduces the functional folding of the glucocorticoid receptor, whereas it reduces only the nuclear translocation of the mineralocorticoid receptor without affecting its function, implying that the effect of HSP90 acetylation on its client proteins is not consistent (Jimenez-Canino et al., 2016). Interestingly, an HSP90 inhibitor reduced the number of PMP22 aggregates by inducing other chaperone proteins, suggesting that the therapeutic potential of HDAC6 inhibitors might come through the acetylation and inhibition of HSP90 function and the induction of PMP22 protein refolding (Rangaraju, Madorsky, Pileggi, Kamal, & Notterpek, 2008). Based on the diverse functions of HDAC6 in protein quality control processes, it was proposed that HDAC6 might contribute to the formation of PMP22 aggregates in CMT1A patients' peripheral neurons and that its inhibition might reduce that formation.

Cytosolic protein aggregates have been considered as the main cause of various neurodegenerative diseases (Eisele et al., 2015). The inhibition of protein aggregates is an emerging target for the treatment of neurodegenerative diseases such as Alzheimer's disease, Parkinson's disease (Davis, Leyns, & Holtzman, 2018), and CMT1A (Rangaraju et al., 2008). In particular, the defective proteasome activity of C22 mice results in PMP22 aggregation and neurodegeneration. The aggregation of proteins induces the endogenous autophagy response. However, autophagy in C22 mice does not seem to be enough to clear the accumulated PMP22 aggregates.

4.5 | The possible mechanism of HDAC6 inhibitor in the regulation of PMP22

There could be several mechanisms underlying the reduction of PMP22 by CKD-504 because HDAC6 is involved in several processes including the induction of aggresome formation, autophagy, and protein refolding (Figure 6f). One possibility is that HDAC6 inhibition induces autophagy and protein aggregate clearance through the lysosomal pathway. In C22 mice, the reduction of PMP22 is probably not be related to autophagy because CKD-504 did not reduce the overall number of ubiquitinated protein aggregates, which indicates that it did not work through the proteasome pathway. In addition, UPR proteins such as CHOP and BiP were induced in the sciatic nerves of C22 mice, and CKD-504 did not affect their expression, indicating that CKD-504 does not regulate the initiation of the UPR (Figure S4E–G). CKD-504 did not affect the gene expression of human PMP22 and murine PMP22 (Figure S4H, I). Another possibility is that the acetylation of HSP90 induces other chaperone proteins to enhance the folding/refolding of PMP22 proteins and enhances the proteasome-mediated degradation of short-lived newly formed PMP22 proteins, which would thus repress the new formation of PMP22 protein aggregates. The observations in this study strongly suggest that CKD-504-mediated PMP22 reduction is due to the last mechanism involved in protein folding/refolding, but that hypothesis should be tested in another study.

Vigo et al. demonstrated that PMP22 overexpression repressed 86 genes involved in the cell cycle, cytoskeletal structure, and extracellular matrix, indicating that the pathogenic mechanism of PMP22 overexpression does not simply stem from misfolded protein-

mediated stress but from altering the signalling cascade of PMP22 (Vigo et al., 2005). They suggested that PMP22 overexpression significantly affects Schwann cell proliferation, differentiation, and function to support the axon, leading to the development of axonal atrophy. Recently, PMP22 protein was found to affect cholesterol trafficking and lipid homeostasis, which are important in myelination (Zhou et al., 2019). In addition, HDAC6 is overexpressed in the lung epithelial cells of cystic fibrosis patients, and it is directly related to an increased cholesterol level in those cells (Lu et al., 2019). An HDAC6 inhibitor was shown to normalize the cholesterol level in the lung epithelial cells of cystic fibrosis patients. Thus, the therapeutic action of CKD-504 could be due to the normalization of lipid homeostasis in Schwann cells.

In this study, we have demonstrated that CKD-504 effectively prevented disease progression and improved function in a mouse model of CMT1A by reducing the expression or aggregation of PMP22. Despite these promising results, several points in this study should be considered. The first issue is whether long-term treatment will produce sustained improvement and prevent further axonal damage. The second issue is whether CKD-504 works in old CMT1A animals and other CMT1A animal models. The third issue is that additional research is required to find an optimal dosing regimen and route. Finally, further study is required to understand the detailed mechanism by which CKD-504 reduces levels of PMP22. Such studies will expand our understanding of the underlying biological mechanism of HDAC6 in neurodegenerative diseases and open a new way to develop effective therapeutic agents for CMT.

4.6 | Clinical development of HDAC6 inhibitors

Although HDAC6 has been proposed as a promising therapeutic target for various diseases, only a few selective HDAC6 inhibitors are available for clinical trials. The well-known genetic and haematological toxicity of the currently available HDAC6 inhibitors has severely limited their potential clinical development for CMT. Therefore, we identified and developed a highly potent and selective HDAC6 inhibitor, CKD-504 (WO2015/137750). In good laboratory practice toxicity studies, CKD-504 did not show any genetic toxicity, and it is now in Phase I clinical trials in the United States (NCT03713892).

In conclusion, CKD-504 reduced PMP22 protein expression and aggregation in the sciatic nerves of CMT1A model mice, improved myelination in vitro, and ameliorated the behavioural, electrophysiological, and pathological features of CMT1A in C22 mice. Therefore, CKD-504 may become a promising therapeutic option for CMT1A.

ACKNOWLEDGEMENTS

We would like to thank the scientists of the Department of Pharmacology, CKD Research Institute for their technical support and assistance. This study was supported by research grants from CKD Pharmaceuticals; the Korean Health Technology R&D Project, Ministry of Health & Welfare (HI14C3484 and HI16C0426); and the National Research Foundation, Republic of Korea (NRF-2016R1A5A2007009, NRF-2017R1A2B2004699, and NRF-2018R1A4A1024506).

AUTHOR CONTRIBUTIONS

N.H., S.C.J., and B.O.C. were responsible for the study design. H.S. synthesized and provided the compound for the experiments. Y.J.L. performed in vitro assays, such as the enzyme kinetics and α-tubulin acetylation assay. J.Y.S., M.C.K., and D.K.B. performed the behavioural and histopathological experiments. N.H. performed histological and molecular biological analyses. N.J., S.J., and S.P. performed experiments with human tonsil-derived mesenchymal stem cells. N.H., Y.I.C., S.C.J., and B.O.C. interpreted the results, contributed to the discussion, and edited the manuscript. All the authors contributed to the interpretation of data and approved the final draft.

CONFLICT OF INTEREST

N.H., Y.I.C., J.Y.S., D.K.B., M.C.K., Y.J.L., and H.S. are employees of CKD Research Institute. The other authors declare no conflict of interest.

DECLARATION OF TRANSPARENCY AND SCIENTIFIC RIGOUR

This declaration acknowledges that this paper adheres to the principles for the transparent reporting and scientific rigour of preclinical research recommended by funding agencies, publishers, and other organizations engaged in supporting research.

REFERENCES

Adalbert, R., Kaieda, A., Antoniou, C., Loreto, A., Yang, X., Gilley, J., … Coleman, M. P. (2020). Novel HDAC6 inhibitors increase tubulin acetylation and rescue axonal transport of mitochondria in a model of Charcot-Marie-Tooth Type 2F. *ACS Chemical Neuroscience*, *11*, 258–267. https://doi.org/10.1021/acschemneuro.9b00338

Alexander, S. P. H., Fabbro, D., Kelly, E., Mathie, A., Peters, J. A., Veale, E. L., … CGTP Collaborators. (2019). THE CONCISE GUIDE TO PHARMACOLOGY 2019/20: Enzymes. *British Journal of Pharmacology*, *176*, S297–S396. https://doi.org/10.1111/bph.14752

Alexander, S. P. H., Kelly, E., Mathie, A., Peters, J. A., Veale, E. L., Faccenda, E., … CGTP Collaborators. (2019). THE CONCISE GUIDE TO PHARMACOLOGY 2019/20: Other Protein Targets. *British Journal of Pharmacology*, *176*, S1–S20. https://doi.org/10.1111/bph.14747

Bali, P., Pranpat, M., Bradner, J., Balasis, M., Fiskus, W., Guo, F., … Bhalla, K. (2005). Inhibition of histone deacetylase 6 acetylates and disrupts the chaperone function of heat shock protein 90: A novel basis for antileukemia activity of histone deacetylase inhibitors. *The Journal of Biological Chemistry*, *280*, 26729–26734. https://doi.org/10.1074/jbc.C500186200

Batchu, S. N., Brijmohan, A. J., & Advani, A. (2016). The therapeutic hope for HDAC6 inhibitors in malignancy and chronic disease. *Clinical Science*, *130*, 987–1003. https://doi.org/10.1042/CS20160084

Bence, N. F., Sampat, R. M., & Kopito, R. R. (2001). Impairment of the ubiquitin-proteasome system by protein aggregation. *Science*, *292*, 1552–1555. https://doi.org/10.1126/science.292.5521.1552

Benoy, V., Van Helleputte, L., Prior, R., d'Ydewalle, C., Haeck, W., Geens, N., … Van Den Bosch, L. (2018). HDAC6 is a therapeutic target in mutant GARS-induced Charcot-Marie-Tooth disease. *Brain*, *141*(3), 673–687. https://doi.org/10.1093/brain/awx375

Benoy, V., Vanden Berghe, P., Jarpe, M., Van Damme, P., Robberecht, W., & Van Den Bosch, L. (2017). Development of improved HDAC6 inhibitors as pharmacological therapy for axonal Charcot-Marie-Tooth disease. *Neurotherapeutics*, *14*, 417–428. https://doi.org/10.1007/s13311-016-0501-z

Boyault, C., Sadoul, K., Pabion, M., & Khochbin, S. (2007). HDAC6, at the crossroads between cytoskeleton and cell signaling by acetylation and ubiquitination. *Oncogene*, *26*, 5468–5476. https://doi.org/10.1038/sj.onc.1210614

Cho, K. A., Kim, J. Y., Kim, H. S., Ryu, K. H., & Woo, S. Y. (2012). Tonsil-derived mesenchymal progenitor cells acquire a follicular dendritic cell phenotype under cytokine stimulation. *Cytokine*, *59*, 211–214. https://doi.org/10.1016/j.cyto.2012.04.016

Curtis, M. J., Alexander, S., Cirino, G., Docherty, J. R., George, C. H., Giembycz, M. A., … Ahluwalia, A. (2018). Experimental design and analysis and their reporting II: Updated and simplified guidance for authors and peer reviewers. *British Journal of Pharmacology*, *175*(7), 987–993. https://doi.org/10.1111/bph.14153

Davis, A. A., Leyns, C. E. G., & Holtzman, D. M. (2018). Intercellular spread of protein aggregates in neurodegenerative disease. *Annual Review of Cell and Developmental Biology*, *34*, 545–568. https://doi.org/10.1146/annurev-cellbio-100617-062636

De Vos, K. J., & Hafezparast, M. (2017). Neurobiology of axonal transport defects in motor neuron diseases: Opportunities for translational research? *Neurobiology of Disease*, *105*, 283–299. https://doi.org/10.1016/j.nbd.2017.02.004

Dompierre, J. P., Godin, J. D., Charrin, B. C., Cordelieres, F. P., King, S. J., Humbert, S., & Saudou, F. (2007). Histone deacetylase 6 inhibition compensates for the transport deficit in Huntington's disease by increasing tubulin acetylation. *The Journal of Neuroscience*, *27*, 3571–3583. https://doi.org/10.1523/JNEUROSCI.0037-07.2007

d'Ydewalle, C., Krishnan, J., Chiheb, D. M., Van Damme, P., Irobi, J., Kozikowski, A. P., … Van Den Bosch, L. (2011). HDAC6 inhibitors reverse axonal loss in a mouse model of mutant HSPB1-induced Charcot-Marie-Tooth disease. *Nature Medicine*, *17*, 968–974. https://doi.org/10.1038/nm.2396

Eisele, Y. S., Monteiro, C., Fearns, C., Encalada, S. E., Wiseman, R. L., Powers, E. T., & Kelly, J. W. (2015). Targeting protein aggregation for the treatment of degenerative diseases. *Nature Reviews. Drug Discovery*, *14*, 759–780. https://doi.org/10.1038/nrd4593

Fiskus, W., Ren, Y., Mohapatra, A., Bali, P., Mandawat, A., Rao, R., … Bhalla, K. (2007). Hydroxamic acid analogue histone deacetylase inhibitors attenuate estrogen receptor-α levels and transcriptional activity: A result of hyperacetylation and inhibition of chaperone function of heat shock protein 90. *Clinical Cancer Research*, *13*, 4882–4890. https://doi.org/10.1158/1078-0432.CCR-06-3093

Fortun, J., Go, J. C., Li, J., Amici, S. A., Dunn, W. A. Jr., & Notterpek, L. (2006). Alterations in degradative pathways and protein aggregation in a neuropathy model based on PMP22 overexpression. *Neurobiology of Disease*, *22*, 153–164. https://doi.org/10.1016/j.nbd.2005.10.010

Fortun, J., Verrier, J. D., Go, J. C., Madorsky, I., Dunn, W. A., & Notterpek, L. (2007). The formation of peripheral myelin protein 22 aggregates is hindered by the enhancement of autophagy and expression of cytoplasmic chaperones. *Neurobiology of Disease*, *25*, 252–265. https://doi.org/10.1016/j.nbd.2006.09.018

Govindarajan, N., Rao, P., Burkhardt, S., Sananbenesi, F., Schluter, O. M., Bradke, F., … Fischer, A. (2013). Reducing HDAC6 ameliorates cognitive deficits in a mouse model for Alzheimer's disease. *EMBO Molecular Medicine*, *5*, 52–63. https://doi.org/10.1002/emmm.201201923

Gregoretti, I. V., Lee, Y. M., & Goodson, H. V. (2004). Molecular evolution of the histone deacetylase family: Functional implications of phylogenetic analysis. *Journal of Molecular Biology*, *338*, 17–31. https://doi.org/10.1016/j.jmb.2004.02.006

Guedes-Dias, P., de Proenca, J., Soares, T. R., Leitao-Rocha, A., Pinho, B. R., Duchen, M. R., & Oliveira, J. M. A. (2015). HDAC6 inhibition induces mitochondrial fusion, autophagic flux and reduces diffuse mutant huntingtin in striatal neurons. *Biochimica et Biophysica Acta*, *1852*, 2484–2493. https://doi.org/10.1016/j.bbadis.2015.08.012

Hanemann, C. O., D'Urso, D., Gabreëls-Festen, A. A., & Müller, H. W. (2000). Mutation-dependent alteration in cellular distribution of peripheral myelin protein 22 in nerve biopsies from Charcot-Marie-Tooth type 1A. *Brain*, *123*, 1001–1006. https://doi.org/10.1093/brain/123.5.1001

Harding, S. D., Sharman, J. L., Faccenda, E., Southan, C., Pawson, A. J., Ireland, S., … NC-IUPHAR. (2018). The IUPHAR/BPS guide to pharmacology in 2018: Updates and expansion to encompass the new guide to immunopharmacology. *Nucleic Acids Research*, *46*, D1091–D1106. https://doi.org/10.1093/nar/gkx1121

Helleputte, L. V., Benoy, V., & Bosch, L. V. D. (2014). The role of histone deacetylase 6 (HDAC6) in neurodegeneration. *Research and Reports in Biology*, *5*, 1–13.

Holzbaur, E. L., & Scherer, S. S. (2011). Microtubules, axonal transport, and neuropathy. *The New England Journal of Medicine*, *365*, 2330–2332. https://doi.org/10.1056/NEJMcibr1112481

Hong, Y. B., Joo, J., Hyun, Y. S., Kwak, G., Choi, Y. R., Yeo, H. K., … Choi, B. O. (2016). A Mutation in PMP2 causes dominant demyelinating Charcot-Marie-Tooth neuropathy. *PLoS Genetics*, *12*, e1005829. https://doi.org/10.1371/journal.pgen.1005829

Huxley, C., Passage, E., Manson, A., Putzu, G., Figarella-Branger, D., Pellissier, J. F., & Fontés, M. (1996). Construction of a mouse model of Charcot-Marie-Tooth disease type 1A by pronuclear injection of human YAC DNA. *Human Molecular Genetics*, *5*, 563–569. https://doi.org/10.1093/hmg/5.5.563

Jimenez-Canino, R., Lorenzo-Diaz, F., Jaisser, F., Farman, N., Giraldez, T., & Alvarez de la Rosa, D. (2016). Histone deacetylase 6-controlled Hsp90 acetylation significantly alters mineralocorticoid receptor subcellular dynamics but not its transcriptional activity. *Endocrinology*, *157*, 2515–2532. https://doi.org/10.1210/en.2015-2055

Johnston, J. A., Ward, C. L., & Kopito, R. R. (1998). Aggresomes: A cellular response to misfolded proteins. *The Journal of Cell Biology*, *143*, 1883–1898. https://doi.org/10.1083/jcb.143.7.1883

Jung, J., Cai, W., Lee, H. K., Pellegatta, M., Shin, Y. K., Jang, S. Y., … Park, H. T. (2011). Actin polymerization is essential for myelin sheath fragmentation during Wallerian degeneration. *The Journal of Neuroscience*, *31*, 2009–2015. https://doi.org/10.1523/JNEUROSCI.4537-10.2011

Jung, N., Park, S., Choi, Y., Park, J. W., Hong, Y. B., Park, H. H., … Jung, S. C. (2016). Tonsil-derived mesenchymal stem cells differentiate into a Schwann cell phenotype and promote peripheral nerve regeneration. *International Journal of Molecular Sciences*, *17*. https://doi.org/10.3390/ijms17111867

Kim, J. Y., Woo, S. Y., Hong, Y. B., Choi, H., Kim, J., Choi, H., … Choi, B.-O. (2016). HDAC6 inhibitors rescued the defective axonal mitochondrial movement in motor neurons derived from the induced pluripotent stem cells of peripheral neuropathy patients with HSPB1 mutation. *Stem Cells International*, *2016*, 9475981.

Kneynsberg, A., Combs, B., Christensen, K., Morfini, G., & Kanaan, N. M. (2017). Axonal degeneration in tauopathies: Disease relevance and underlying mechanisms. *Frontiers in Neuroscience*, *11*, 572. https://doi.org/10.3389/fnins.2017.00572

Kovacs, J. J., Murphy, P. J., Gaillard, S., Zhao, X., Wu, J. T., Nicchitta, C. V., … Yao, T.-P. (2005). HDAC6 regulates Hsp90 acetylation and chaperone-dependent activation of glucocorticoid receptor. *Molecular Cell*, *18*, 601–607. https://doi.org/10.1016/j.molcel.2005.04.021

Krukowski, K., Ma, J., Golonzhka, O., Laumet, G. O., Gutti, T., van Duzer, J. H., … Kavelaars, A. (2017). HDAC6 inhibition effectively reverses chemotherapy-induced peripheral neuropathy. *Pain*, *158*(6), 1126–1137. https://doi.org/10.1097/j.pain.0000000000000893

Lee, S., Amici, S., Tavori, H., Zeng, W. M., Freeland, S., Fazio, S., & Notterpek, L. (2014). PMP22 is critical for actin-mediated cellular functions and for establishing lipid rafts. *The Journal of Neuroscience*, *34*, 16140–16152. https://doi.org/10.1523/JNEUROSCI.1908-14.2014

Lee, S., Bazick, H., Chittoor-Vinod, V., Al Salihi, M. O., Xia, G., & Notterpek, L. (2018). Elevated peripheral myelin protein 22, reduced mitotic potential, and proteasome impairment in dermal fibroblasts from Charcot-Marie-Tooth disease type 1A patients. *The American Journal of Pathology*, *188*, 728–738. https://doi.org/10.1016/j.ajpath.2017.10.021

Lilley, E., Stanford, S. C., Kendall, D. E., Alexander, S. P., Cirino, G., Docherty, J. R., … Ahluwalia, A. (2020). ARRIVE 2.0 and the *British Journal of Pharmacology*: Updated guidance for 2020. *British Journal of Pharmacology*. https://doi.org/10.1111/bph.15178

Lu, B., Li, L., Schneider, M., Hodges, C. A., Cotton, C. U., Burgess, J. D., & Kelley, T. J. (2019). Electrochemical measurement of membrane cholesterol correlates with CFTR function and is HDAC6-dependent. *Journal of Cystic Fibrosis*, *18*, 175–181. https://doi.org/10.1016/j.jcf.2018.06.005

Ma, J., Trinh, R. T., Mahant, I. D., Peng, B., Matthias, P., Heijnen, C. J., & Kavelaars, A. (2019). Cell-specific role of histone deacetylase 6 in chemotherapy-induced mechanical allodynia and loss of intraepidermal nerve fibers. *Pain*, *160*, 2877–2890. https://doi.org/10.1097/j.pain.0000000000001667

Millecamps, S., & Julien, J. P. (2013). Axonal transport deficits and neurodegenerative diseases. *Nature Reviews. Neuroscience*, *14*, 161–176. https://doi.org/10.1038/nrn3380

Mo, Z., Zhao, X., Liu, H., Hu, Q., Chen, X. Q., Pham, J., … Yang, X. L. (2018). Aberrant GlyRS-HDAC6 interaction linked to axonal transport deficits in Charcot-Marie-Tooth neuropathy. *Nature Communications*, *9*, 1007–1017. https://doi.org/10.1038/s41467-018-03461-z

Notterpek, L., Ryan, M. C., Tobler, A. R., & Shooter, E. M. (1999). PMP22 accumulation in aggresomes: Implications for CMT1A pathology. *Neurobiology of Disease*, *6*, 450–460. https://doi.org/10.1006/nbdi.1999.0274

Ouyang, H., Ali, Y. O., Ravichandran, M., Dong, A., Qiu, W., MacKenzie, F., … Zhai, R. G. (2012). Protein aggregates are recruited to aggresome by histone deacetylase 6 via unanchored ubiquitin C termini. *The Journal of Biological Chemistry*, *287*, 2317–2327. https://doi.org/10.1074/jbc.M111.273730

Pandey, U. B., Nie, Z., Batlevi, Y., McCray, B. A., Ritson, G. P., Nedelsky, N. B., … Taylor, J. P. (2007). HDAC6 rescues neurodegeneration and provides an essential link between autophagy and the UPS. *Nature*, *447*, 859–863. https://doi.org/10.1038/nature05853

Pareyson, D., Saveri, P., & Pisciotta, C. (2017). New developments in Charcot-Marie-Tooth neuropathy and related diseases. *Current Opinion in Neurology*, *30*, 471–480. https://doi.org/10.1097/WCO.0000000000000474

Park, S., Choi, Y., Jung, N., Yu, Y., Ryu, K. H., Kim, H. S., … Jung, S.-C. (2016). Myogenic differentiation potential of human tonsil-derived mesenchymal stem cells and their potential for use to promote skeletal muscle regeneration. *International Journal of Molecular Medicine*, *37*, 1209–1220. https://doi.org/10.3892/ijmm.2016.2536

Park, S., Jung, N., Myung, S., Choi, Y., Chung, K. W., Choi, B. O., & Jung, S. C. (2018). Differentiation of human tonsil-derived mesenchymal stem cells into Schwann-like cells improves neuromuscular function in a mouse model of Charcot-Marie-Tooth disease type 1A. *International Journal of Molecular Sciences*, *19*. https://doi.org/10.3390/ijms19082393

Prior, R., Van Helleputte, L., Benoy, V., & Van Den Bosch, L. (2017). Defective axonal transport: A common pathological mechanism in inherited and acquired peripheral neuropathies. *Neurobiology of Disease*, *105*, 300–320. https://doi.org/10.1016/j.nbd.2017.02.009

Percie du Sert, N., Hurst, V., Ahluwalia, A., Alam, S., Avey, M. T., Baker, M., … Würbel, H. (2020). The ARRIVE guidelines 2.0: Updated guidelines for reporting animal research. *PLoS Biology*, *18*(7), e3000410. https://doi.org/10.1371/journal.pbio.3000410

Rangaraju, S., Madorsky, I., Pileggi, J. G., Kamal, A., & Notterpek, L. (2008). Pharmacological induction of the heat shock response improves myelination in a neuropathic model. *Neurobiology of Disease*, *32*, 105–115. https://doi.org/10.1016/j.nbd.2008.06.015

Rimando, M. G., Wu, H. H., Liu, Y. A., Lee, C. W., Kuo, S. W., Lo, Y. P., … Lee, O. K. S. (2016). Glucocorticoid receptor and histone deacetylase 6 mediate the differential effect of dexamethasone during osteogenesis of mesenchymal stromal cells (MSCs). *Scientific Reports*, *6*, 37371. https://doi.org/10.1038/srep37371

Rossaert, E., & Van Den Bosch, L. (2020). HDAC6 inhibitors: Translating genetic and molecular insights into a therapy for axonal CMT. *Brain Research*, *29*, 146692–146703.

de Ruijter, A. J., van Gennip, A. H., Caron, H. N., Kemp, S., & van Kuilenburg, A. B. (2003). Histone deacetylases (HDACs): Characterization of the classical HDAC family. *The Biochemical Journal*, *370*, 737–749. https://doi.org/10.1042/bj20021321

Ryan, M. C., Shooter, E. M., & Notterpek, L. (2002). Aggresome formation in neuropathy models based on peripheral myelin protein 22 mutations. *Neurobiology of Disease*, *10*, 109–118. https://doi.org/10.1006/nbdi.2002.0500

Saibil, H. (2013). Chaperone machines for protein folding, unfolding and disaggregation. *Nature Reviews. Molecular Cell Biology*, *14*, 630–642. https://doi.org/10.1038/nrm3658

Scherer, S. S., & Chance, P. F. (1995). Myelin genes: Getting the dosage right. *Nature Genetics*, *11*, 226–228. https://doi.org/10.1038/ng1195-226

Scroggins, B. T., Robzyk, K., Wang, D., Marcu, M. G., Tsutsumi, S., Beebe, K., … Neckers, L. (2007). An acetylation site in the middle domain of Hsp90 regulates chaperone function. *Molecular Cell*, *25*, 151–159. https://doi.org/10.1016/j.molcel.2006.12.008

Seidel, C., Schnekenburger, M., Dicato, M., & Diederich, M. (2015). Histone deacetylase 6 in health and disease. *Epigenomics*, *7*, 103–118. https://doi.org/10.2217/epi.14.69

Selenica, M., Benner, L., Housely, S. B., Manchec, B., Lee, D. C., Nash, K. R., & Morgan, D. (2014). Histone deacetylase 6 inhibition improves memory and reduces total tau levels in a mouse model of tau deposition. *Alzheimer's Research & Therapy*, *6*, 12. https://doi.org/10.1186/alzrt241

Shan, B., Yao, T. P., Nguyen, H. T., Zhuo, Y., Levy, D. R., Klingsberg, R. C., … Lasky, J. A. (2008). Requirement of HDAC6 for transforming growth factor-β1-induced epithelial-mesenchymal transition. *The Journal of Biological Chemistry*, *283*, 21065–21073. https://doi.org/10.1074/jbc.M802786200

Shin, Y. K., Jang, S. Y., Park, S. Y., Park, J. Y., Kim, J. K., Kim, J. P., … Park, H. T. (2014). Grb2-associated binder-1 is required for neuregulin-1-induced peripheral nerve myelination. *The Journal of Neuroscience*, *34*, 7657–7662. https://doi.org/10.1523/JNEUROSCI.4947-13.2014

Simoes-Pires, C., Zwick, V., Nurisso, A., Schenker, E., Carrupt, P. A., & Cuendet, M. (2013). HDAC6 as a target for neurodegenerative diseases: What makes it different from the other HDACs? *Molecular Neurodegeneration*, *8*, 7. https://doi.org/10.1186/1750-1326-8-7

Skre, H. (1974). Genetic and clinical aspects of Charcot-Marie-Tooth's disease. *Clinical Genetics*, *6*, 98–118. https://doi.org/10.1111/j.1399-0004.1974.tb00638.x

Skultetyova, L., Ustinova, K., Kutil, Z., Novakova, Z., Pavlicek, J., Mikesova, J., … Barinka, C. (2017). Human histone deacetylase 6 shows strong preference for tubulin dimers over assembled microtubules. *Scientific Reports*, *7*, 11547. https://doi.org/10.1038/s41598-017-11739-3

Taes, I., Timmers, M., Hersmus, N., Bento-Abreu, A., Van Den Bosch, L., Van Damme, P., … Robberecht, W. (2013). Hdac6 deletion delays disease progression in the SOD1G93A mouse model of ALS. *Human Molecular Genetics*, *22*, 1783–1790. https://doi.org/10.1093/hmg/ddt028

Tao, H., Yang, J. J., Hu, W., Shi, K. H., & Li, J. (2016). HDAC6 promotes cardiac fibrosis progression through suppressing RASSF1A expression. *Cardiology*, *133*, 18–26. https://doi.org/10.1159/000438781

Timmerman, V., Strickland, A. V., & Zuchner, S. (2014). Genetics of Charcot-Marie-Tooth (CMT) disease within the frame of the human genome project success. *Genes (Basel)*, *5*, 13–32. https://doi.org/10.3390/genes5010013

Tsuji, G., Okiyama, N., Villarroel, V. A., & Katz, S. I. (2015). Histone deacetylase 6 inhibition impairs effector CD8 T-cell functions during skin inflammation. *The Journal of Allergy and Clinical Immunology*, *135*, 1228–1239. https://doi.org/10.1016/j.jaci.2014.10.002

Van Hellelputte, L., Kater, M., Cook, D. P., Eykens, C., Rossaert, E., Haeck, W., … Van Den Bosch, L. (2018). Inhibition of histone deacetylase 6 (HDAC6) protects against vincristine-induced peripheral neuropathies and inhibits tumor growth. *Neurobiology of Disease*, *111*, 59–69. https://doi.org/10.1016/j.nbd.2017.11.011

Vigo, T., Nobbio, L., Hummelen, P. V., Abbruzzese, M., Mancardi, G., Verpoorten, N., … Schenone, A. (2005). Experimental Charcot-Marie-Tooth type 1A: A cDNA microarrays analysis. *Molecular and Cellular Neurosciences*, *28*, 703–714. https://doi.org/10.1016/j.mcn.2004.11.016

Wegener, D., Wirsching, F., Riester, D., & Schwienhorst, A. (2003). A fluorogenic histone deacetylase assay well suited for high-throughput activity screening. *Chemistry & Biology*, *10*, 61–68. https://doi.org/10.1016/S1074-5521(02)00305-8

Xu, L., Liu, N., Gu, H., Wang, H., Shi, Y., Ma, X., … Zhuang, S. (2017). Histone deacetylase 6 inhibition counteracts the epithelial-mesenchymal transition of peritoneal mesothelial cells and prevents peritoneal fibrosis. *Oncotarget*, *8*, 88730–88750. https://doi.org/10.18632/oncotarget.20982

Yan, J., Seibenhener, M. L., Calderilla-Barbosa, L., Diaz-Meco, M. T., Moscat, J., Jiang, J., … Wooten, M. C. (2013). SQSTM1/p62 interacts with HDAC6 and regulates deacetylase activity. *PLoS ONE*, *8*, e76016. https://doi.org/10.1371/journal.pone.0076016

Youn, G. S., Cho, H., Kim, D., Choi, S. Y., & Park, J. (2017). Crosstalk between HDAC6 and Nox2-based NADPH oxidase mediates HIV-1 Tat-induced pro-inflammatory responses in astrocytes. *Redox Biology*, *12*, 978–986. https://doi.org/10.1016/j.redox.2017.05.001

Zhang, Y., Kwon, S., Yamaguchi, T., Cubizolles, F., Rousseaux, S., Kneissel, M., … Matthias, P. (2008). Mice lacking histone deacetylase 6 have hyperacetylated tubulin but are viable and develop normally. *Molecular and Cellular Biology*, *28*, 1688–1701. https://doi.org/10.1128/MCB.01154-06

Zhao, R., & Houry, W. A. (2005). Hsp90: A chaperone for protein folding and gene regulation. *Biochemistry and Cell Biology*, *83*, 703–710. https://doi.org/10.1139/o05-158

Zhou, Y., Miles, J. R., Tavori, H., Lin, M., Khoshbouei, H., Borchelt, D. R., … Notterpek, L. (2019). PMP22 regulates cholesterol trafficking and ABCA1-mediated cholesterol efflux. *The Journal of Neuroscience*, *39*, 5404–5418. https://doi.org/10.1523/JNEUROSCI.2942-18.2019

Zilberman, Y., Ballestrem, C., Carramusa, L., Mazitschek, R., Khochbin, S., & Bershadsky, A. (2009). Regulation of microtubule dynamics by inhibition of the tubulin deacetylase HDAC6. *Journal of Cell Science*, *122*, 3531–3541. https://doi.org/10.1242/jcs.046813

SUPPORTING INFORMATION

Additional supporting information may be found online in the Supporting Information section at the end of this article.

How to cite this article: Ha N, Choi YI, Jung N, et al. A novel histone deacetylase 6 inhibitor improves myelination of Schwann cells in a model of Charcot–Marie–Tooth disease type 1A. *Br J Pharmacol*. 2020;177:5096–5113. https://doi.org/10.1111/bph.15231